

REFERENCE COPY

# SANDIA REPORT

SAND90-3246 • UC-721

Unlimited Release

Printed June 1991



SAND90-3246  
0002  
UNCLASSIFIED

06/91  
62P

STAC

## Evaluation of the Role of Threshold Pressure in Controlling Flow of Waste-Generated Gas into Bedded Salt at the Waste Isolation Pilot Plant

Peter B. Davies

Prepared by  
Sandia National Laboratories  
Albuquerque, New Mexico 87185 and Livermore, California 94550  
for the United States Department of Energy  
under Contract DE-AC04-76DP00789

Issued by Sandia National Laboratories, operated for the United States Department of Energy by Sandia Corporation.

**NOTICE:** This report was prepared as an account of work sponsored by an agency of the United States Government. Neither the United States Government nor any agency thereof, nor any of their employees, nor any of their contractors, subcontractors, or their employees, makes any warranty, express or implied, or assumes any legal liability or responsibility for the accuracy, completeness, or usefulness of any information, apparatus, product, or process disclosed, or represents that its use would not infringe privately owned rights. Reference herein to any specific commercial product, process, or service by trade name, trademark, manufacturer, or otherwise, does not necessarily constitute or imply its endorsement, recommendation, or favoring by the United States Government, any agency thereof or any of their contractors or subcontractors. The views and opinions expressed herein do not necessarily state or reflect those of the United States Government, any agency thereof or any of their contractors.

Printed in the United States of America. This report has been reproduced directly from the best available copy.

Available to DOE and DOE contractors from  
Office of Scientific and Technical Information  
PO Box 62  
Oak Ridge, TN 37831  
Prices available from (615) 576-8401, FTS 626-8401

Available to the public from  
National Technical Information Service  
US Department of Commerce  
5285 Port Royal Rd  
Springfield, VA 22161  
NTIS price codes  
Printed copy: A04  
Microfiche copy: A01

SAND90-3246  
Unlimited Release  
Printed June 1991

Distribution  
Category UC-721

## **EVALUATION OF THE ROLE OF THRESHOLD PRESSURE IN CONTROLLING FLOW OF WASTE-GENERATED GAS INTO BEDDED SALT AT THE WASTE ISOLATION PILOT PLANT**

Peter B. Davies  
Fluid Flow and Transport Division 6344  
Sandia National Laboratories  
Albuquerque, New Mexico

### **ABSTRACT**

Anoxic corrosion and microbial degradation of contact-handled transuranic waste may produce sufficient quantities of gas over a long time period to generate high pressure in the disposal rooms at the Waste Isolation Pilot Plant (WIPP) repository. Dissipation of pressure by outward gas flow will be inhibited by the low permeability of the surrounding rock and by capillary forces that resist gas penetration into this water-saturated rock. Threshold pressure is the gas pressure required to overcome capillary resistance to initial gas penetration and to the development of interconnected gas pathways that would allow outward gas flow. The primary objectives of this study are to estimate the magnitude of threshold pressure in the bedded salt that surrounds the WIPP repository and to evaluate the role this parameter plays in controlling the outward flow of waste-generated gas. Estimates of threshold pressure have been made based on an empirical correlation of threshold pressure with intrinsic permeability from other low-permeability rock types and on a capillary tube model. These two approaches yield generally consistent estimates, suggesting that threshold pressure in relatively pure halite is 20 to 50 MPa, or larger; threshold pressure in impure halite is 5 to 25 MPa; and threshold pressure in more permeable nonhalite interbeds is 2 to 1/2 MPa, or less. Because of the compounding effect of low threshold pressure and relatively high permeability, the nonhalite interbeds are likely to be the dominant pathways for flow of waste-generated gas away from a pressurized repository. Near the repository, a number of processes occur that may significantly

reduce threshold pressure. Local fracturing and pore dilatation in response to excavation-related stresses creates larger pore apertures. Desaturation occurs as a result of drying, dilatation, and/or exsolution of gas that is dissolved in Salado brine under natural conditions. All of these processes contribute to the development of a zone surrounding the repository that contains pore space that is readily accessible to waste-generated gas due to significantly decreased threshold pressures. The threshold pressure estimates and analyses presented in this report are based primarily on threshold pressure information from low-permeability, nonsalt rock types and must be confirmed with direct, laboratory, and/or in situ measurements specific to the Salado Formation at the WIPP repository. In particular, such measurements should be directed toward the nonhalite interbeds and impure halite.

## **ACKNOWLEDGMENTS**

The author thanks Geoff Freeze, Bob Glass, and Elaine Gorham for their helpful review comments on this report. The author also appreciates review and subsequent discussions of a preliminary version of this report with Rick Beauheim, Susan Howarth, Marsh LaVenue, Dave McTigue, John Pickens, and Steve Webb. Carol Gotway provided helpful guidance in the analysis of uncertainty in the correlation of threshold pressure and intrinsic permeability.



## CONTENTS

<b>1.</b>	<b>INTRODUCTION</b>	<b>1</b>
<b>2.</b>	<b>THEORETICAL BACKGROUND ON THRESHOLD PRESSURE</b>	<b>7</b>
<b>3.</b>	<b>TECHNIQUES FOR MEASURING THRESHOLD PRESSURE</b>	<b>13</b>
3.1	Direct Measurements	13
3.2	Indirect Measurements	13
<b>4.</b>	<b>TECHNIQUES FOR ESTIMATING THRESHOLD PRESSURE</b>	<b>17</b>
4.1	Empirical Correlations	17
4.2	Capillary Tube Model	20
<b>5.</b>	<b>THRESHOLD PRESSURE ESTIMATES FOR THE SALADO FORMATION</b>	<b>25</b>
5.1	Estimates Based on Permeability Correlation	25
5.2	Estimates Based on Capillary Tube Model	29
<b>6.</b>	<b>OTHER PROCESSES AND PHYSICAL CHARACTERISTICS THAT MAY INFLUENCE THRESHOLD PRESSURE IN THE WIPP ENVIRONMENT</b>	<b>31</b>
6.1	Threshold Pressure Under Partially Saturated Conditions	31
6.2	Impact of Fracturing on Threshold Pressure	32
6.3	Possibility of Zero Permeability in Undeformed, Pure Halite	33
<b>7.</b>	<b>DISCUSSION</b>	<b>35</b>
7.1	Threshold Pressure Estimates for the Salado Formation	35
7.2	Conceptual Model for Hydrologic Response of the Repository to Waste-Generated Gas	37
<b>8.</b>	<b>REFERENCES</b>	<b>39</b>

## FIGURES

1.	Definition of relative permeability to water (brine) and gas as a function of the degree of water (or gas) saturation . . . . .	3
2.	Schematic illustration of the role of threshold pressure in inhibiting gas flow from a gas-filled disposal room into adjacent low-permeability rock that is brine saturated . . . . .	4
3.	Definition of threshold pressure and relationship between capillary pressure and relative permeability . . . . .	11
4.	Plot showing an example of threshold pressure measurement by mercury injection for a 1 microdarcy ( $10^{-18}$ m <sup>2</sup> ) sandstone . . . . .	14
5.	Plot of threshold pressure versus intrinsic permeability for a wide variety of geologic materials and over a 13 order-of-magnitude range in intrinsic permeability . . . . .	18
6.	Plot of estimated versus measured threshold pressure for estimates based on the capillary tube model . . . . .	22
7.	Plot of estimation error versus intrinsic permeability for threshold pressure estimates based on empirical correlation and on the capillary tube model . . . . .	23
8.	Plot of correlation of threshold pressure with intrinsic permeability for a composite of data from all consolidated rock lithologies . . . . .	26
9.	Plot summarizing estimated threshold pressure for various lithologic units in the Salado Formation based on correlation with intrinsic permeability . . . . .	28

## TABLES

1.	Highest observed fluid pressures in the Salado Formation . . . . .	2
2.	Range of threshold pressure parameters for geologic systems . . . . .	10
3.	Threshold pressure versus intrinsic permeability correlations . . . . .	19
4.	Parameter values for estimating threshold pressure of the Salado Formation (far-field) based on the capillary tube model . . . . .	30



## 1. INTRODUCTION

Analyses of the post-closure evolution of disposal rooms in the Waste Isolation Pilot Plant (WIPP) repository indicate that microbial degradation of organic waste and anoxic corrosion of steel drums and metallic waste may be capable of generating enough gas to pressurize the rooms to lithostatic pressure (Lappin et al., 1989). Recent estimates of gas generation by anoxic corrosion suggest a production rate of 2 moles/drum per year with a total potential of 900 moles/drum (Brush, 1990). Similar estimates for gas generation by microbial activity suggest a production rate of 1 mole/drum per year with a total potential of 600 moles. Gas generation by radiolysis is expected to proceed at a much slower rate. Current gas-generation research is focused on laboratory and in situ experiments that will provide a more accurate prediction of gas-generation rates under brine-inundated conditions and of possible rate reductions under vapor-limited ("humid") conditions. Other in situ measurements and model analyses focus on assessing the hydrologic and mechanical response of the disposal rooms and surrounding Salado Formation to high gas pressure.

An important objective in assessing the hydrologic response to waste-generated gas is determining how much gas can flow from the repository into the surrounding rock mass, thereby regulating gas pressure within the repository. Three physical characteristics of the surrounding rock will control the flow of gas from the repository into the rock. These characteristics are pore fluid pressure, threshold pressure, and gas permeability.

The difference between fluid pressure in pores of the waste and backfill in the repository and fluid pressure in the pores of the surrounding Salado Formation provides the primary driving force for moving gas and brine between these two regions. Current measurements indicate that undisturbed (i.e. far-field) pore pressure in the Salado Formation at the elevation of the repository is between hydrostatic (5.9 MPa) and lithostatic (14.8 MPa) (Peterson et al., 1987; Nowak and McTigue, 1987; Lappin et al., 1989). Highest pore pressures are usually measured in anhydrite interbeds and range from 8.8 to 11.5 Mpa (Table 1). Pore pressures extrapolated from pressure recovery trends yield higher values, ranging from 9.3 to 13.9 MPa (Table 1). Pore pressures are much lower within the first few meters of the excavation surface due to depressurization that accompanies brine flow toward the excavation and/or to dilatation of pores caused by high deviatoric stresses near the excavation.

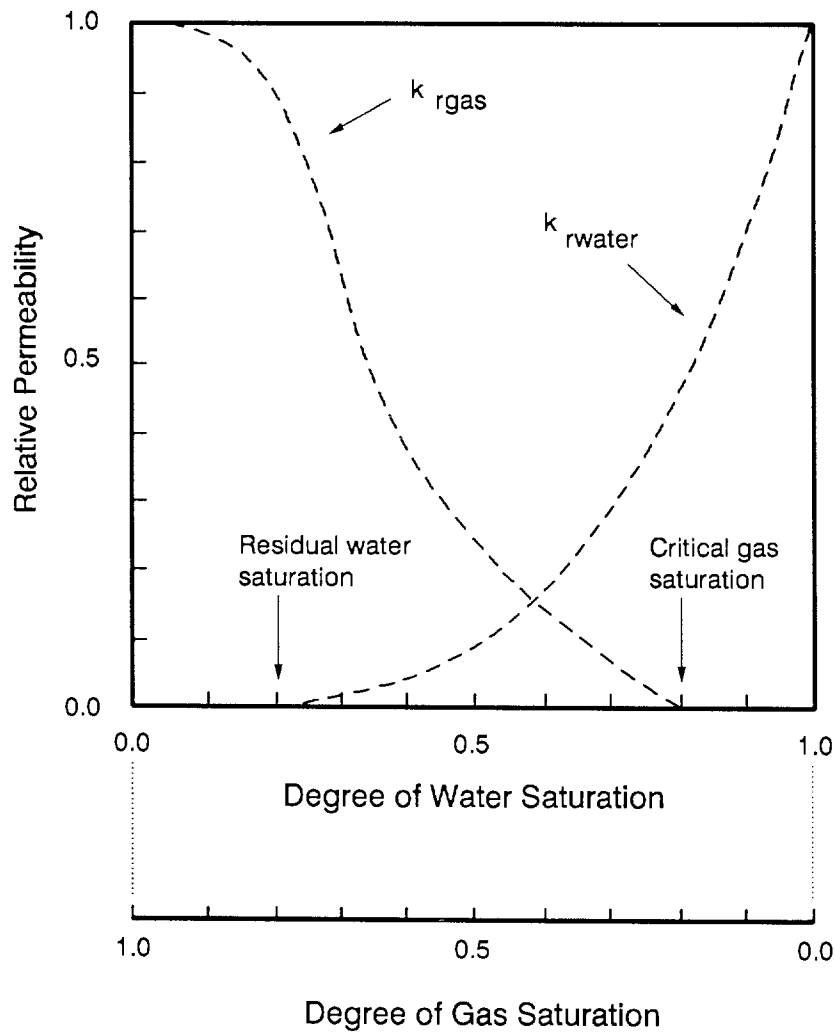
The second characteristic controlling gas flow into the rock is the threshold pressure required to overcome capillary resistance and drive gas into the brine-filled rock pores. Rock that is fully saturated with brine is impermeable to gas (Figure 1) until the capillary forces resisting the penetration of gas into the rock pores have been overcome and a network of interconnected gas pathways has been established. The sum of the existing pore pressure in the rock and the threshold pressure is the gas-pressure level that must be reached in the room before gas can flow from the room into the rock (Figure 2). Because the rock is depressurized within the first few meters of an excavation, the pore-pressure component of this sum will be relatively small. However, for gas penetration beyond the first few meters, the pore-pressure component of this sum is much larger, on the order of 12 MPa or higher as discussed in the previous paragraph.

**Table 1. Highest observed fluid pressures in the Salado Formation.**

LITHOLOGIC UNIT	DISTANCE FROM EXCAVATION (m)	APPROXIMATE AGE OF EXCAVATION (yr)	HIGHEST MEASURED PRESSURE (MPa)	HIGHEST EXTRAPOLATED PRESSURE (MPa)	REFERENCE
Marker Bed 139	12	2 3/4	10.3	10.3	Peterson et al., 1987
Marker Bed 139	10	5 1/2	8.8	9.3	Beauheim et al., in review
Marker Bed 139	23	1/2	10.5	10.7 - 12.8	Howarth et al., in press
Anhydrite B	22	1/2	11.5	12.8	Howarth et al., in press
Marker Bed 138	24	1/2	9.3	9.3 - 13.9	Howarth et al., in press

The third characteristic controlling the flow of gas from the repository is the permeability of the rock to gas. Gas permeability is a function of the intrinsic permeability of the rock and of the degree of saturation, which controls the relative permeability to gas and brine (Figure 1). When little or no gas is present, the gas phase is not continuous throughout the pore network and, therefore, no interconnected gas flow pathways exist. In this state, the rock is impermeable to gas. Only after sufficient gas is present to create interconnected pathways does the rock become permeable to gas. The fluid saturation corresponding to the incipient development of an interconnected network of gas pathways is commonly referred to as the critical gas saturation or residual equilibrium gas saturation (Figure 1). As gas saturation increases further, relative permeability to gas becomes larger and relative permeability to brine becomes smaller. At high gas saturations, a point is eventually reached where brine is no longer continuous throughout the pore network and relative permeability to brine becomes zero. This point is commonly referred to as the residual water saturation. At high gas saturations, the relative permeability to gas approaches 1.0 and in this state the permeability of the rock to gas approaches the intrinsic permeability.

The physical characteristics of the rock and fluid surrounding the WIPP repository are complex. The Salado Formation contains interbeds of clay and anhydrite, which in situ tests indicate have much higher permeability than the halite (Beauheim et al., in review; Howarth et al., in press).



Definitions:

$$k_{r\text{gas}} = \frac{k_{\text{gas}}}{k}$$

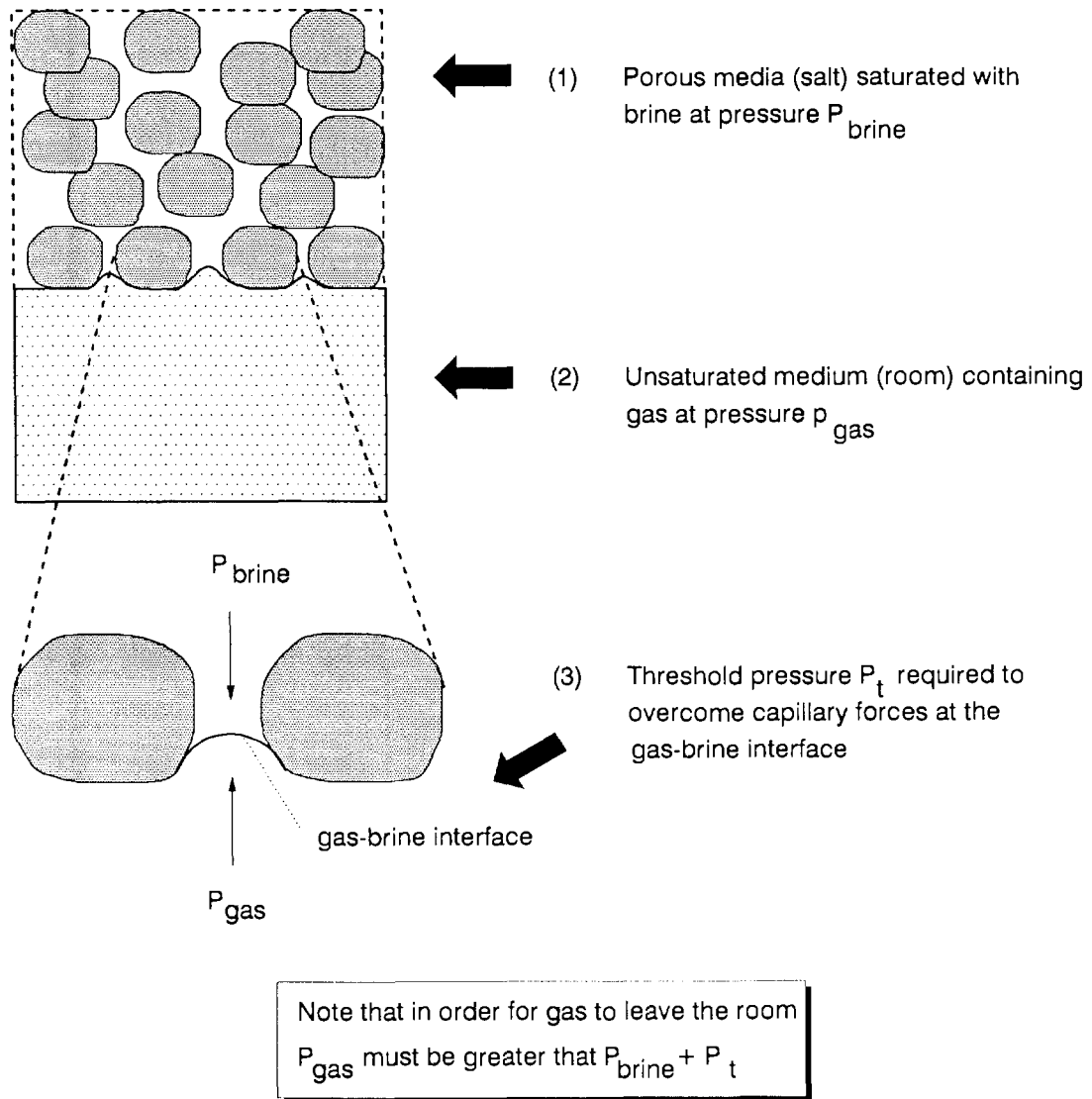
$$k_{r\text{water}} = \frac{k_{\text{water}}}{k}$$

$k$  = intrinsic permeability to a single-phase fluid that completely saturates the medium

Note that at water saturations between the critical gas saturation and 1.0, the rock is impermeable to gas

TRI-6344-723-0

Figure 1. Definition of relative permeability to water (brine) and gas as a function of the degree of water (or gas) saturation. Also note definitions of residual water saturation and critical gas saturation.



TRI-6344-724-0

Figure 2. Schematic illustration of the role of threshold pressure in inhibiting gas flow from a gas-filled disposal room into adjacent low-permeability rock that is brine saturated.

The halite itself contains stratigraphic variations in grain size, texture, and impurity content (mostly clay). In situ tests, laboratory measurements, and brine seepage observations indicate that hydraulic characteristics of the halite units are also variable. In addition to natural variability in the Salado Formation, stress redistribution in response to excavation of the repository has caused near-field changes in hydrologic conditions: dilatation and fracturing have increased intrinsic rock permeability in some locations; brine drainage has decreased pore pressures in the Salado; elastic and inelastic changes in pore volume have caused additional complexity in the near-field fluid pressure distribution; and dilatation, drying, and possible exsolution of dissolved gas that occurs naturally in the Salado brine have caused varying degrees of desaturation (Borns and Stormont, 1988, 1989; Nowak and McTigue, 1897; McTigue et al., 1989; Stormont et al., 1987).

At the June, 1989 National Academy of Sciences WIPP Panel Meeting, John Bredehoeft (U.S. Geological Survey) and George Hornberger (University of Virginia) suggested that because threshold pressure is controlled to a large degree by pore size and because pores in halite are extremely small, threshold pressure may be extremely high. Therefore, the combination of high existing pore pressures and high threshold pressures may create a situation in which the rock surrounding the WIPP repository is effectively impermeable to gas. Concern was expressed that in the absence of gas flow from the repository, pressures may reach or exceed lithostatic and cause fracturing of unpredictable orientation and extent.

As a first step toward assessing potential for gas flow out of the WIPP repository, the objectives of this study are to estimate the magnitude of threshold pressure in the bedded salt that surrounds the WIPP repository and to characterize the role that threshold pressure may play in controlling the outward flow of waste-generated gas. In order to accomplish these objectives, the following discussion is divided into three main segments. The first segment focuses on threshold pressure theory and techniques for measuring and estimating threshold pressure in low permeability environments. The second segment focuses on estimates of threshold pressure for the Salado Formation in the vicinity of the WIPP repository. The third segment focuses on other processes and physical characteristics that may influence threshold pressure in the WIPP environment.



## 2. THEORETICAL BACKGROUND ON THRESHOLD PRESSURE

When two immiscible fluids such as water and gas are in contact, a discontinuity in pressure exists across the interface that separates them. Water, which tends to adhere to the rock matrix, is referred to as the wetting phase, while the gas constitutes the nonwetting phase. The difference in pressure between these two fluids is called capillary pressure  $p_c$ :

$$p_c = p_{\text{gas}} - p_{\text{water}} \quad (1)$$

Capillary pressure is a function of the effective radius  $r_e$  of the rock pores, surface tension  $\sigma$  along the interface, and the contact angle  $\alpha$  between the interface and the adjacent solid material:

$$p_c = \frac{2 \sigma \cos \alpha}{r_e} \quad (2)$$

Effective radius,  $r_e$ , is defined in terms of principle radii  $r_1$  and  $r_2$ , and therefore, is affected by both pore size and pore shape:

$$\frac{2}{r_e} = \left( \frac{1}{r_1} + \frac{1}{r_2} \right) \quad (3)$$

In most analyses involving water with glass or rock, complete wetting of the solid is assumed. Under these conditions,  $\cos \alpha$  is equal to one and Equation (2) becomes:

$$p_c = \frac{2 \sigma}{r_e} \quad (4)$$

In order for gas to penetrate a fluid-filled capillary tube or a saturated porous material, pressure in the gas must be high enough to deform the interface to a sufficiently small radius to pass through the tube or rock pores. Pore space in rock is actually a complex arrangement of space with relatively large effective radius, "pores," and space with relatively small effective radius, "necks." Gas penetration into a water-saturated rock is controlled to a large degree by the small effective radius pore space, that is by the necks. In low-permeability rock, the effective radius of necks is very small, and therefore the gas pressure required to overcome capillary forces and permit gas penetration is very large.

One approach to quantifying threshold pressure phenomena in porous media has been to develop an idealized model using a bundle of capillary tubes as the conceptual framework. Based on Poiseuille's Law for laminar flow through an individual capillary tube, Darcy's Law for flow through porous media, and the relationship between capillary pressure and tube radius, the following expression for threshold pressure can be derived (Wyllie and Spangler, 1952; Thomas et al., 1968):

$$P_t = \sigma \left[ \frac{T \phi}{k_0 k} \right]^{1/2} \quad (5)$$

where:

$P_t$  = threshold pressure [M/LT<sup>2</sup>]

$\sigma$  = surface tension [M/T<sup>2</sup>]

$\phi$  = porosity [dimensionless]

$k_0$  = pore shape factor [dimensionless]

$T$  = tortuosity [dimensionless]

$k$  = intrinsic permeability [L<sup>2</sup>]

Tortuosity is a measure of the actual length of tortuous flow pathways in a porous medium and is defined in the hydrology literature as follows (Bear, 1972):

$$T = \left[ \frac{L}{L_e} \right]^2 \quad (6)$$

where:

$L$  = length of porous system [L]

$L_e$  = length of tortuous flow path through porous system [L]

In order to avoid confusion, it should be noted that the definition of tortuosity in the petroleum literature is the reciprocal of Equation 6 (Rose and Bruce, 1949; Wyllie and Spangler, 1952).

The variation of measured parameter values in Equation 5 is summarized in Table 2 for gas-water systems in geologic settings ranging from unsaturated flow in unconsolidated materials near the ground surface to natural gas reservoirs at depth. By far the dominant parameter controlling threshold pressure over this broad range of geologic environments is intrinsic permeability, which has a range spanning approximately 13 orders of magnitude. Both the capillary model represented by Equation 5 and empirical correlations of threshold pressure versus intrinsic permeability have been widely used in the petroleum industry to make estimates of threshold pressure (Thomas et al., 1968; Katz and Coates, 1968; Katz and Tek, 1970; Ibrahim et al., 1970). These estimation techniques will be discussed in more detail in a later section of this report.

Studies of threshold-pressure phenomena have utilized a variety of techniques to measure nonwetting-phase penetration pressures and a variety of terminology has been applied (Dullien, 1979). In some instances, the definition of threshold pressure contains different assumptions about what constitutes initial "penetration" or "breakthrough" of gas or some other nonwetting phase. Natural materials contain pores of many different sizes and flow along any given pathway may encounter both large radii pores and small radii necks. On a microscopic scale, gas will penetrate into larger pores at lower capillary pressure than is required for penetration through smaller pores or necks with relatively small effective radii. Some investigators define threshold pressure as the capillary pressure associated with first penetration of a nonwetting phase into the largest pores near the surface of the medium. Others define threshold pressure as the capillary pressure associated with the incipient development of a continuum of the nonwetting phase through a pore network, providing gas pathways not only through relatively large pores, but also through necks between pores.

The physical distinction between these two definitions of threshold pressure is illustrated in Figure 3, which shows the relationship between capillary pressure under draining conditions and the corresponding changes in relative permeability to the gas and water phases. Defining threshold pressure as corresponding to first penetration of a nonwetting phase into the largest pores near the surface of the medium means that threshold pressure is equal to the capillary pressure at a water saturation of 1.0. Defining threshold pressure as corresponding to the incipient formation of a continuum of the nonwetting phase through the pore network means that threshold pressure is equal to the capillary pressure at a saturation equal to the critical gas saturation. In other words, threshold pressure is equal to the capillary pressure at which the relative permeability to the gas phase begins to rise from its zero value, corresponding to the incipient development of interconnected gas flow paths through the pore network.

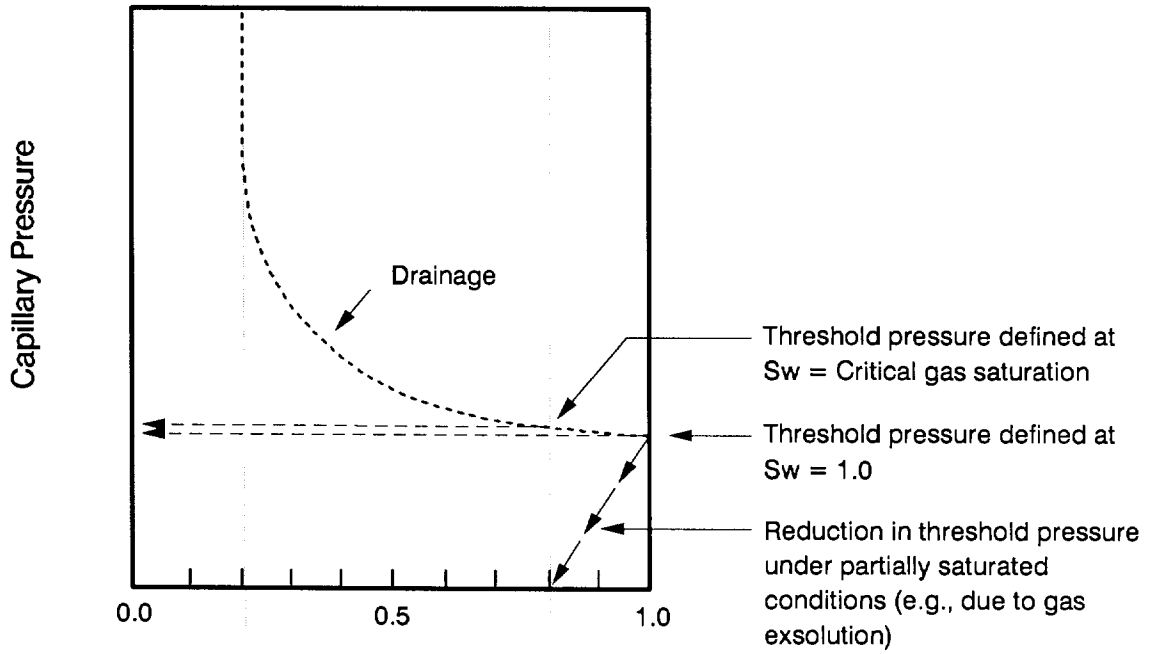
The present study is concerned with the potential for flow of waste-generated gas outward from the WIPP repository. This process will likely require that outward flowing gas penetrate and establish a gas-filled network of flow paths in the surrounding bedded salt. Therefore, the latter definition of threshold pressure being associated with the incipient formation of a continuous network of gas flow paths has been adopted for this study.

**Table 2. Range of threshold pressure parameters for geologic systems.**

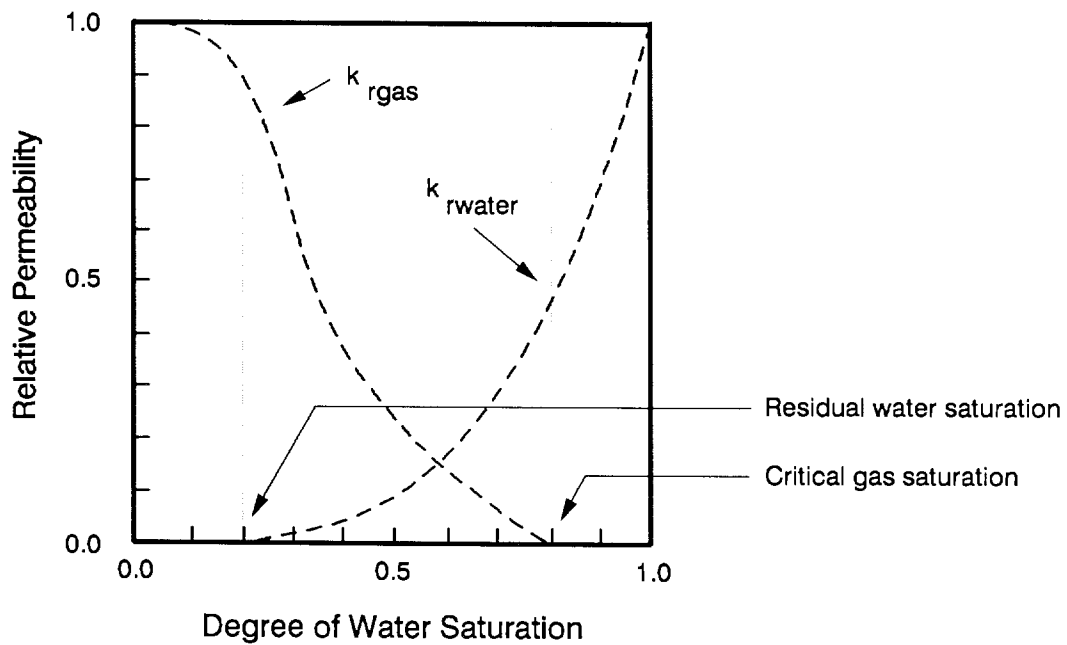
PARAMETER	RANGE	COMMENTS	MAGNITUDE OF RANGE	REFERENCE
Surface tension	Low	0.05 N/m	1.6	Hocott, 1939
	High	0.08 N/m		
Porosity	Low	0.001	500	Powers et al., 1978
	High	0.500		
Pore shape factor	Low	2.0	1.5	Wyllie and Spangler, 1952
	High	3.0		
Tortuosity	Low	0.02	35	Barker and Foster, 1981
	High	0.70		
Permeability	Low	$10^{-22} \text{ m}^2$	$10^{13}$	Nowak et al., 1988; Ibrahim et al., 1970
	High	$10^{-9} \text{ m}^2$		

As noted previously, threshold pressure phenomena have been studied in a broad range of geologic environments. Studies of unsaturated flow, commonly in high- to intermediate-permeability soils, have used threshold pressure (commonly referred to as "bubbling pressure" or "air-entry pressure" in the unsaturated flow literature) as an indirect measure of the equivalent diameter of the largest neck in a given sample and as a fundamental hydraulic parameter for characterizing unsaturated materials (Brooks and Corey, 1964; Stakman, 1968; Cosby et al., 1984). Studies of oil and gas reservoirs, in a wide range of rock types, have used threshold pressure to characterize the role of capillary pressure in trapping petroleum fluids and in influencing multiphase fluid response to pumping (Hassler et al., 1943; Muskat, 1949; Hubbert, 1953). Studies of underground storage of natural gas (Thomas et al., 1968; Ibrahim et al., 1970) and other fluids such as compressed air (Katz and Lady, 1976) and hydrogen (Carden and Paterson, 1979) have examined threshold pressures in low

### Capillary Pressure



### Relative Permeability



TRI-6344-725-0

Figure 3. Definition of threshold pressure and relationship between capillary pressure and relative permeability.

to very low-permeability rock in great detail because capillary sealing in the caprock is of critical importance for successful underground storage of gases. These very low-permeability caprock environments are similar in many respects to the very low-permeability environment in the salt surrounding the WIPP repository. Therefore, the following discussions of threshold pressure measurement and estimation draw primarily from research directed toward underground gas storage.

### **3. TECHNIQUES FOR MEASURING THRESHOLD PRESSURE**

Research on threshold pressure in caprocks for underground gas storage reservoirs has produced a variety of techniques for measuring threshold pressures in low-permeability materials. Laboratory measurements of threshold pressure can be divided into two categories: direct measurements and indirect measurements. To date, no techniques for in situ measurement of threshold pressure have been reported.

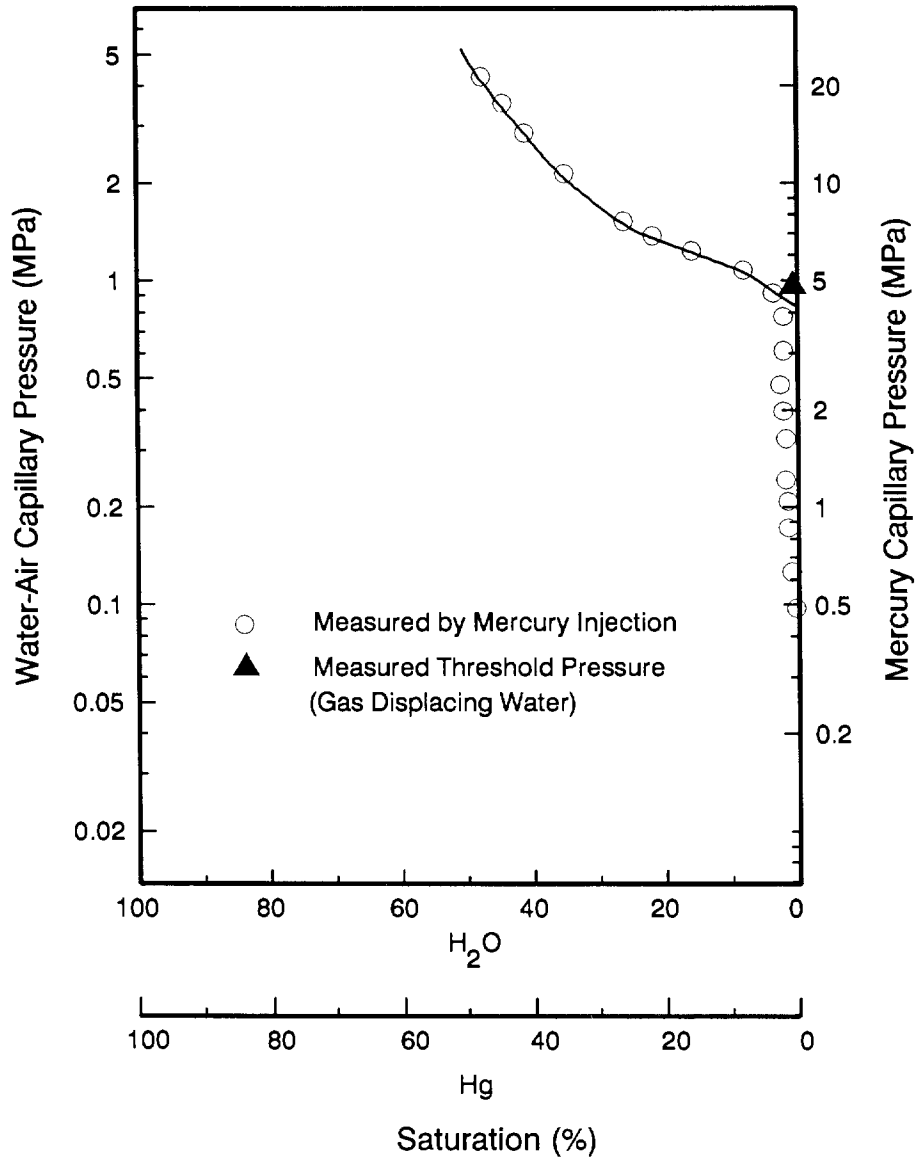
#### **3.1 Direct Measurements**

Threshold pressure can be measured directly by incrementally increasing the pressure of gas in contact with the end of a fully saturated core sample and observing the pressure at which gas first penetrates through the core. This approach measures the pressure required for the incipient development of interconnected gas flow paths through the pore network. Direct measurement techniques were first developed by Thomas et al. (1968) and were later enhanced by Ibrahim et al. (1970) and Pandey et al. (1973). In addition to threshold pressure, intrinsic permeability is commonly measured on the same core prior to the threshold pressure measurement. Using these techniques, threshold pressures as high as 14 MPa and intrinsic permeabilities as low as  $9 \times 10^{-23} \text{ m}^2$  (approximately 0.1 nanodarcy) have been measured on low-permeability caprock materials (Ibrahim et al., 1970). Caprock lithologies exhibiting high threshold pressures and low permeabilities include anhydrite, carbonate, and shale. No measurements of threshold pressure in bedded salt have been reported in the literature.

#### **3.2 Indirect Measurements**

The second category of threshold pressure measurements is based on extrapolating measurements of capillary pressure versus saturation to capillary pressure at a water saturation equal to 1.0. This approach measures the pressure required to initiate gas penetration into the largest pores near the surface of the medium. This technique has been used for a broad range of materials, from high-permeability unconsolidated materials (Brooks and Corey, 1964; Stakman, 1968; Cosby et al., 1984) to low-permeability caprocks (Thomas et al., 1968; Ibrahim et al., 1970). While measurement of the capillary pressure curve in higher permeability materials can be carried out by direct measurements of suction pressure as an initially water-saturated sample is dried, measurement of the capillary pressure curve in low-permeability materials is more difficult.

One technique for measuring capillary pressure curves in low-permeability materials is to measure progressive mercury injection into a dry core sample at successively higher injection pressures (Figure 4). Extrapolation to air-water conditions is accomplished by multiplying by the appropriate capillary pressure ratio for water versus mercury systems (Purcell, 1949; Thomas et al., 1968). A second technique for measuring capillary pressure curves in low-permeability materials is to estimate the pore-size distribution (expressed as effective pore radius) by measuring adsorption of



TRI-6344-726-0

Figure 4. Plot showing an example of threshold pressure measurement by mercury injection for a 1 microdarcy ( $10^{-18} \text{ m}^2$ ) sandstone. (Figure adapted from Thomas et al., 1968, Figure 6.)

nitrogen gas in a dry sample (Ibrahim et al., 1970). The corresponding capillary pressure curve is then computed using the relationship between capillary pressure and pore radius expressed in Equation 4. A third technique for measuring capillary pressure curves in low-permeability materials is based on the theoretical relationship between capillary pressure and vapor pressure in the vicinity of a curved vapor-liquid interface (Saito, 1963; Ibrahim et al., 1970). For this technique, vapor pressure in a sealed flask containing a core sample is measured as the degree of saturation is decreased in successive steps. Capillary pressures are then calculated from the theoretical capillary-pressure and vapor-pressure relationship.

Comparison of threshold pressure determinations by direct versus indirect techniques has yielded consistency between techniques to within approximately one-half order of magnitude, or better, for most samples (Thomas et al., 1968; Ibrahim et al., 1970). The dominant approach for determining threshold pressures in low-permeability rock is by direct measurement. An advantage of the direct approach is that intrinsic permeability is readily measured using the same equipment, making acquisition of this important parameter a routine component of the total procedure. An advantage of the indirect technique is that it produces the entire capillary pressure curve, which is also an important piece of information in multiphase flow analysis.



## 4. TECHNIQUES FOR ESTIMATING THRESHOLD PRESSURE

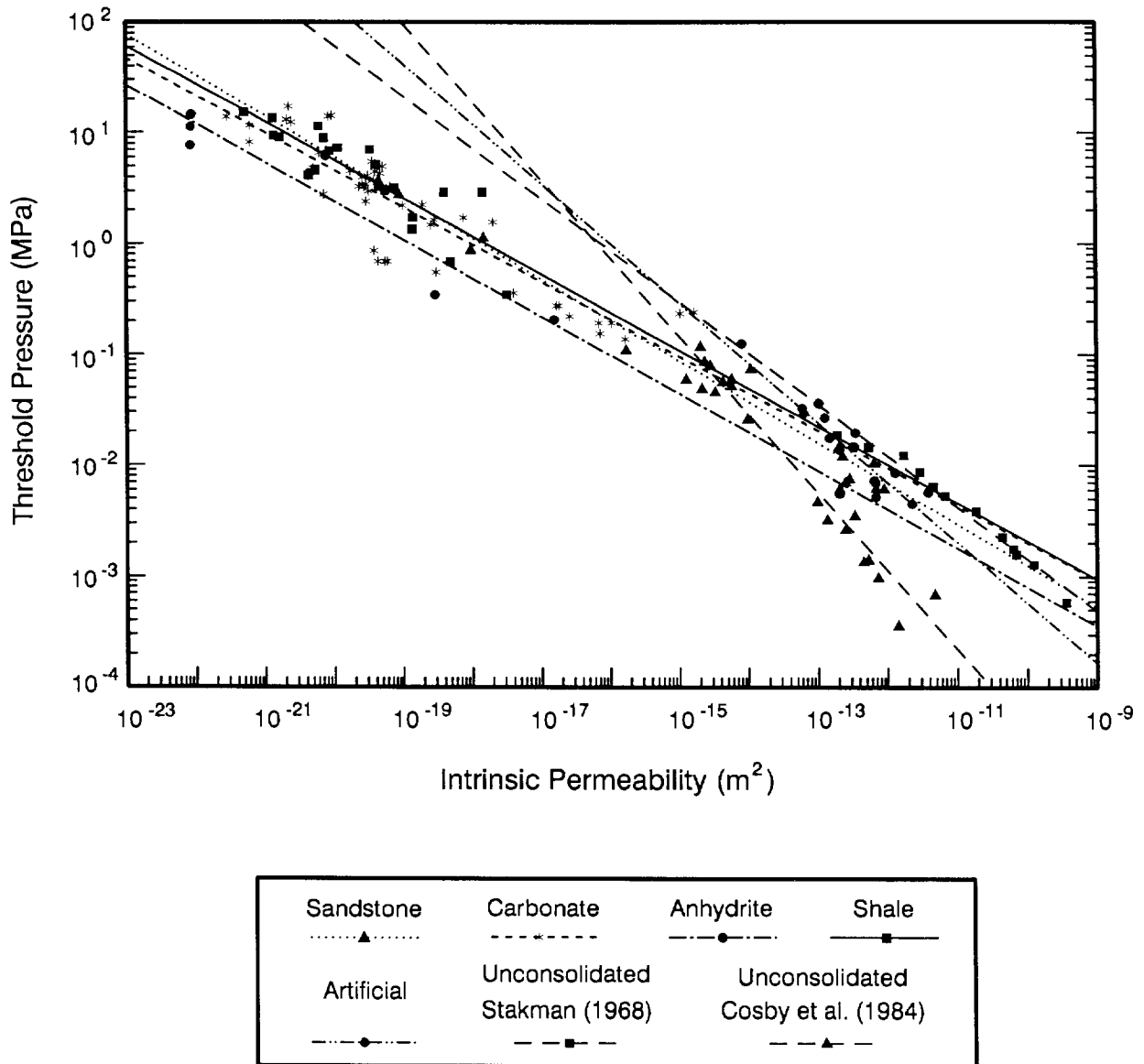
Because laboratory measurement of threshold pressure requires carefully controlled conditions and significant analytic effort, techniques for estimating threshold pressure have been developed as well. Two approaches to threshold pressure estimation have been developed, one based on empirical correlation and the other based on the capillary tube model described in Section 2. In this report and where it appears in the threshold pressure literature, the term "empirical correlation" is used as a general description for an empirical model (describing the relationship between threshold pressure and intrinsic permeability) rather than as a specific statistical quantity associated with correlation coefficients.

### 4.1 Empirical Correlations

Correlations of threshold pressure with intrinsic permeability have been presented in the soils literature for unconsolidated materials (Stakman, 1968) and in the petroleum literature for consolidated rock (Thomas et al., 1968; Ibrahim et al., 1970). The physical rationale behind this approach is that both threshold pressure and intrinsic permeability are strongly related to pore size and pore interconnections in some fashion. As noted in the previous discussion of the capillary tube model, over the broad spectrum of geologic environments, intrinsic permeability ranges over 13 orders of magnitude (Table 2) and is the dominant factor controlling threshold pressure. The parameter with the second largest range (2-1/2 orders of magnitude) is porosity. Empirical correlations for threshold pressure that incorporate both intrinsic permeability and porosity have also been tested, but show no significant improvement in fit over correlations that use only intrinsic permeability (Ibrahim, 1970).

A detailed literature review has yielded threshold pressure and intrinsic permeability data for a broad range of lithologies with permeabilities ranging from approximately  $1 \times 10^{-9}$  to  $1 \times 10^{-22} \text{ m}^2$  (1000 darcies to 0.1 nanodarcy). Most data at the lower end of this range come from measurements on caprock lithologies associated with underground gas storage research. Data at the high end of this range are primarily from unconsolidated soils and artificial porous media. Figure 5 is a plot of threshold pressure versus intrinsic permeability, grouped by lithology. This plot contains only data from research laboratory measurements carried out under carefully controlled conditions. Data from commercial laboratories were not included because of the frequent absence of lithologic information and uncertainty in the range of quality control in the measurements. Data from Cosby et al. (1984) for unconsolidated materials have been presented as a separate curve because these data represent mean values from a large number of samples in groups of different textural classifications rather than individual sample points.

The empirical correlations presented in Figure 5 and summarized in Table 3 reveal a distinct similarity in threshold-pressure versus intrinsic-permeability relationships for the consolidated



TRI-6344-727-0

Figure 5. Plot of threshold pressure versus intrinsic permeability for a wide variety of geologic materials and over a 13 order-of-magnitude range in intrinsic permeability. Data references are summarized in Table 3.

**Table 3. Threshold pressure versus intrinsic permeability correlations.**

LITHOLOGIC GROUP	NUMBER OF SAMPLES	EXPONENT <sup>(1)</sup> (b)	COEFFICIENT <sup>(1)</sup> (a)	GOODNESS-OF-FIT (R <sup>2</sup> )	DATA REFERENCES
<b>CONSOLIDATED LITHOLOGIES</b>					
Carbonate	49	-0.336	$8.7 \times 10^{-7}$	0.80	Thomas et al., 1968; Ibrahim et al., 1970
Anhydrite	7	-0.348	$2.6 \times 10^{-7}$	0.90	Ibrahim et al., 1970
Shale	22	-0.344	$7.6 \times 10^{-7}$	0.74	Ibrahim et al., 1970
Sandstone	22	-0.369	$2.5 \times 10^{-7}$	0.97	Thomas et al., 1968; Wyllie & Rose, 1950; Rose and Bruce, 1949
<b>OTHER LITHOLOGIES</b>					
Unconsolidated (2)	11	-0.706	$3.7 \times 10^{-12}$	0.65	Cosby et al., 1984
Unconsolidated (3)	12	-0.464	$3.3 \times 10^{-8}$	0.97	Stakman, 1968
Artificial	18	-0.540	$2.3 \times 10^{-9}$	0.81	Wyllie & Rose, 1950; Rose and Bruce, 1949
<b>COMPOSITE OF CONSOLIDATED LITHOLOGIES</b>					
	100	-0.346	$5.6 \times 10^{-7}$	0.93	
<b>FOOTNOTES:</b>					
(1) Exponent (b) and coefficient (a) refer to Equation 7.					
(2) Data are mean values for a large number of samples in groups of different soil textural classification.					
(3) Data are actual values for sand samples sorted by grain size.					

lithologies, which include sandstone, shale, carbonate, and anhydrite. These data have been fit with a power curve of the form:

$$y = a x^b \quad (7)$$

The best fit power curves for these lithologies are quite similar, with exponents ranging from -0.34 to -0.37 and coefficients ranging from  $3 \times 10^{-7}$  to  $9 \times 10^{-7}$ . On the other hand, the curves for the high permeability lithologies (unconsolidated soils and artificial porous media) are different, with exponents ranging from -0.46 to -0.71 and coefficients ranging from  $3 \times 10^{-8}$  to  $3 \times 10^{-12}$ . The exponents for the best fit power curves for all lithologies are generally similar to the theoretical -0.50 exponent indicated by the capillary tube model (Equation 5). The Stakman (1968) data for sorted sand are characterized by a close fit ( $R^2$  is equal to 0.97) and by an exponent (-0.46) that is quite similar to the theoretical -0.50 value. Exponents for the consolidated lithologies are all close to -0.35, suggesting that factors other than intrinsic permeability may exert secondary influence on the correlation for consolidated materials.

## 4.2 Capillary Tube Model

A second approach to estimating threshold pressure is based on the capillary tube model (Equation 5) that explicitly incorporates the influence of additional parameters beyond intrinsic permeability. An objective of Thomas et al. (1968) in developing the capillary tube model for threshold pressure was to develop a model in which all of the parameters are readily measured. Of the parameters in the capillary tube model expressed in Equation 5, only pore shape factor and tortuosity cannot be measured directly. Because the pore shape parameter appears as a square root in Equation 5 and its expected range is very small compared to other parameters (Table 2), this parameter has little impact on calculated threshold pressures.

While tortuosity cannot be measured directly, it can be determined indirectly using electrical resistivity measurements. The tortuous path length,  $L_e$ , of fluid flow can be indirectly measured by measuring the flow of electrical current along the same path (Wyllie and Spangler, 1952; Calhoun, 1953; Katz et al., 1957). In a porous medium saturated with a conducting fluid such as brine, the flow of electrical current is almost entirely through the fluid with negligible flow through the solid matrix. Since electrical current is conducted only through the fluid within the porous medium, the resistivity of a saturated sample is higher than the resistivity of the fluid alone. The ratio between the resistivity of a fully saturated porous medium to the resistivity of the saturating fluid is called the "formation factor,"  $F$ . Because the flow of electricity is analogous to the flow of a fluid with zero viscosity, pore diameters do not affect electrical current flow. Therefore, formation factor depends only on flow path length and porosity (Wyllie and Spangler, 1952):

$$F = \frac{\rho_s}{\rho_l} = \frac{1}{\phi} \left[ \frac{L_e}{L} \right] \quad (8)$$

where:

$\rho_s$  = resistivity of saturated porous media

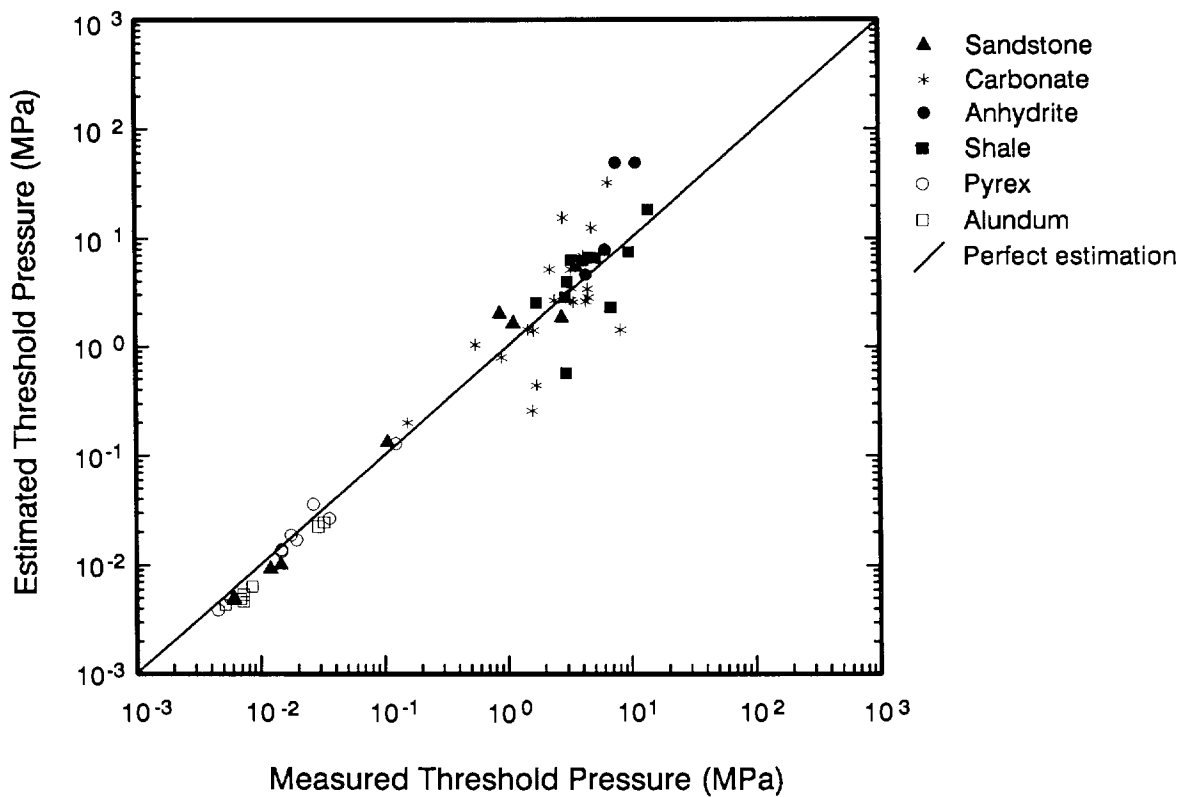
$\rho_l$  = resistivity of the saturating liquid

Bear (1972) has derived a relation between formation factor and tortuosity that differs somewhat from the relation implied by Equations 6 and 8. The Wyllie and Spangler (1952) relation is used here for consistency with the original derivation of the capillary tube model by Thomas et al. (1968).

Using formation factor as a measure of tortuosity, Equations 6 and 8 are substituted into the capillary pressure model expressed in Equation 5 to yield an expression for threshold pressure in which all significant parameters are readily measurable (Thomas et al., 1968):

$$P_t = \frac{\sigma}{F} \left[ \frac{1}{k_0 \phi k} \right]^{1/2} \quad (9)$$

Use of Equation 9 requires a more extensive suite of data than is required for the threshold-pressure versus intrinsic-permeability correlations and, therefore, fewer data are available for testing this model than are available for the empirical correlations. Figure 6 is a plot of estimated versus measured threshold pressures for the capillary tube model. Data for this plot are from four consolidated rock types (sandstone, shale, anhydrite, and carbonate) and two artificial porous materials (pyrex and alundum). The data span intrinsic permeabilities from approximately  $10^{-12}$  to  $10^{-22} \text{ m}^2$  (1 darcy to 0.1 nanodarcy) and measured threshold pressures ranging from approximately  $5 \times 10^{-3}$  to  $1.4 \times 10^1$  MPa. For materials with threshold pressures less than about 1 MPa, estimations based on the capillary tube model are quite accurate. Estimations are less accurate for materials with threshold pressures greater than 1 MPa. Six samples have estimated threshold pressures that are above 10 MPa. For all of these samples, measured threshold pressure is less than the estimated value. This discrepancy could reflect difficulties in measuring threshold pressures that exceed 10 MPa or larger uncertainties in the associated measurements of very low permeability (less than  $10^{-20} \text{ m}^2$ ). Alternatively, this discrepancy, and perhaps the wider scatter above 1 MPa, could reflect changes in the pore structure or interactions between pore fluid and pore walls in very tight materials that are not accounted for in the capillary tube model.



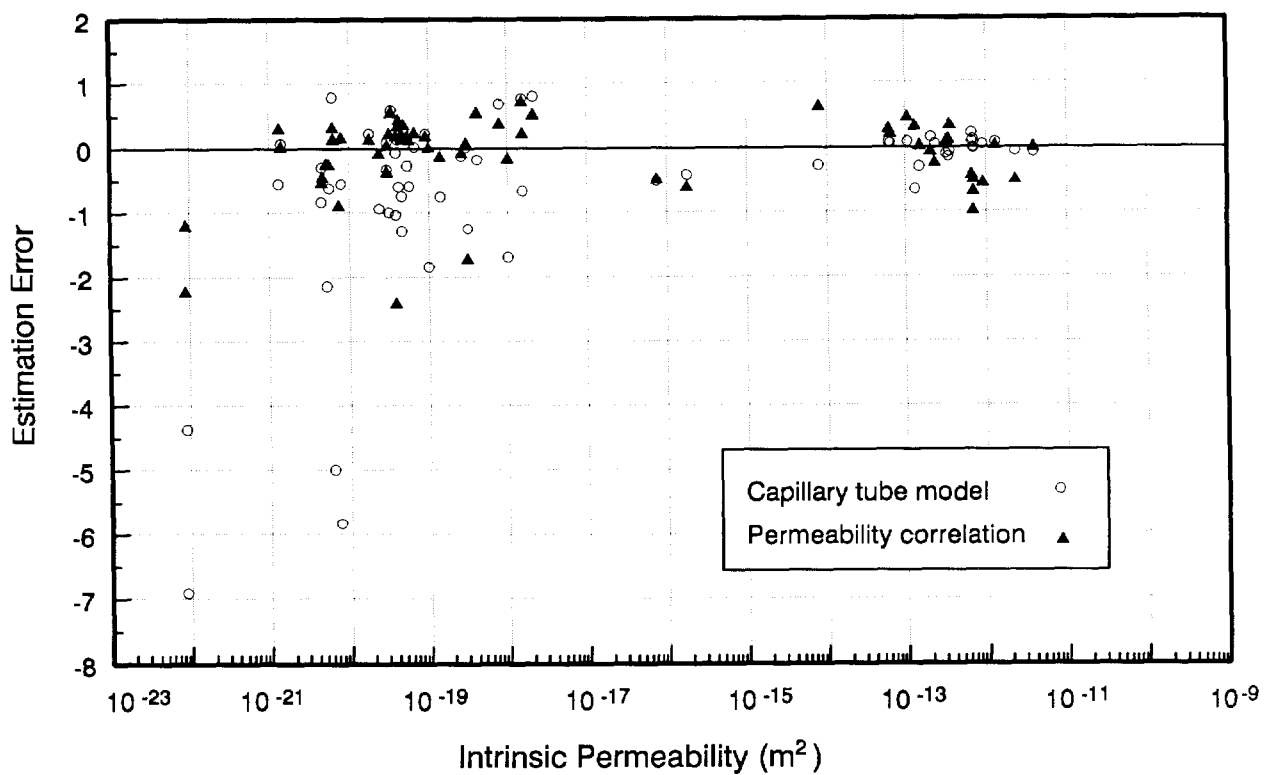
TRI-6344-728-0

Figure 6. Plot of estimated versus measured threshold pressure for estimates based on the capillary tube model. Data are from Thomas et al. (1968), Wyllie and Rose (1950), and Ibrahim et al. (1970).

Because threshold pressure estimations based on the capillary tube model appear to be less accurate at the low permeability end of the range, a comparison of the relative accuracy of estimations based on intrinsic permeability correlations versus estimations based on the capillary tube model has been carried out. For this comparison, estimation error has been defined as follows:

$$P_{t-error} = \frac{P_{t-measured} - P_{t-estimated}}{P_{t-measured}} \tag{10}$$

Figure 7 is a plot of estimation error as a function of intrinsic permeability. This plot illustrates that for samples with permeability greater than  $10^{-17} \text{m}^2$ , both methods produce estimation errors less than 1. In this permeability range, the capillary tube model produces somewhat more accurate estimations. For samples with permeability less than  $10^{-17} \text{m}^2$ , both methods produce larger estimation errors, with a tendency to significantly overestimate threshold pressure in some samples. At this low permeability end of the range, estimations based on the intrinsic permeability correlation appear to be more accurate.



$$\text{Estimation error} = (P_{t \text{ measured}} - P_{t \text{ estimated}}) / P_{t \text{ measured}}$$

TRI-6344-729-0

Figure 7. Plot of estimation error versus intrinsic permeability for threshold pressure estimates based on empirical correlation and on the capillary tube model.



## 5. THRESHOLD PRESSURE ESTIMATES FOR THE SALADO FORMATION

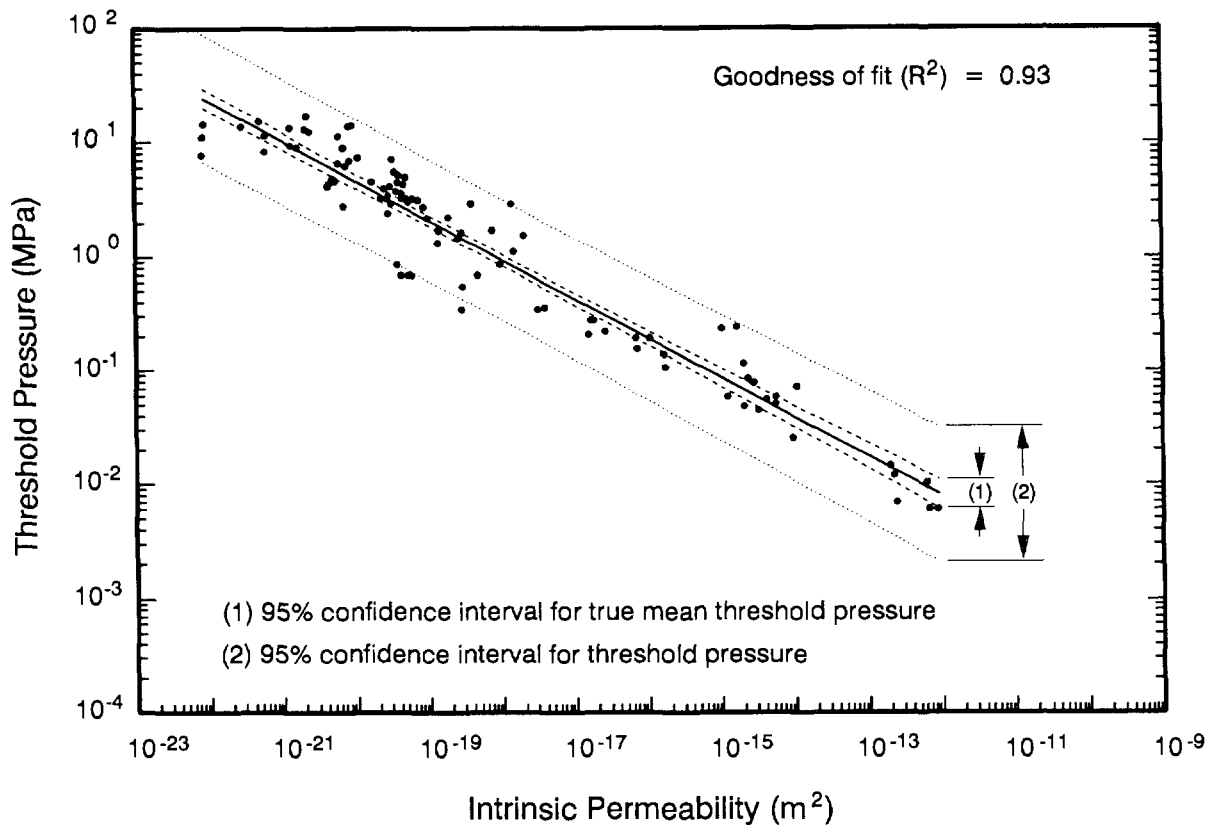
As noted previously, threshold pressure may be an important parameter controlling the flow of waste-generated gas into the rock surrounding the waste-disposal rooms at the WIPP repository. Based on a model of rock pores as uniform tubes and estimates of pore apertures, Stormont et al. (1987) estimated that the threshold pressure for intact halite is somewhere in the range from 100 to less than 1 MPa. In order to further evaluate this parameter for the WIPP environment, estimates of its magnitude have been made using the techniques described in previous sections of this report and existing knowledge of the physical characteristics of the Salado Formation.

### 5.1 Estimates Based on Permeability Correlation

The Salado Formation, which consists of thick halite beds with anhydrite and clay interbeds, is similar in many respects to the consolidated lithologies presented in Figure 5. Halite, anhydrite, and low-permeability carbonates are all characterized by relatively tight crystalline textures with interconnected pore space occurring along grain boundaries and possibly associated with small fractures. Low-permeability sandstones may also have similarities in pore structure, with crystalline cements filling much of the original open intergrain pore space. The pore structure of clay interbeds of the Salado is expected to be generally similar to that of shales, with platy clay minerals aligned parallel to bedding planes. Given these general similarities, a best-fit power curve through the combined data set for consolidated lithologies was judged to provide the best available correlation for providing estimates of threshold pressure for the Salado Formation (Figure 8; Table 3). This correlation yields the following relationship between threshold pressure and intrinsic permeability:

$$P_t (MPa) = 5.6 \times 10^{-7} [k (m^2)]^{-0.346} \quad (11)$$

Permeability measurements in the Salado Formation have been the focus of significant effort over the course of the WIPP project. In order to address the inherent difficulties in measuring permeability in such tight rock, measurement techniques have evolved over time with significant improvements in both accuracy and lower limits of resolution. Most of the early measurements made in deep boreholes from the ground surface have subsequently been determined to be unreliable because of poorly defined pretest conditions and/or problems with analytic techniques (Lappin et al., 1989; Beauheim et al., in review). In the one surface-based test considered reliable, only an upper bound on the composite permeability of the Marker Bed 138 to Marker Bed 139 interval ( $< 3 \times 10^{-19} m^2$ ) was determined (Beauheim, 1986). Given the difficulties with surface-based measurements, efforts in recent years have focused exclusively on tests in holes drilled directly into the Salado Formation from the WIPP shafts and underground workings.



TRI-6344-730-0

Figure 8. Plot of correlation of threshold pressure with intrinsic permeability for a composite of data from all consolidated rock lithologies. Data are from Ibrahim et al., 1970; Rose and Bruce, 1949; Thomas et al., 1968; and Wyllie and Rose, 1950.

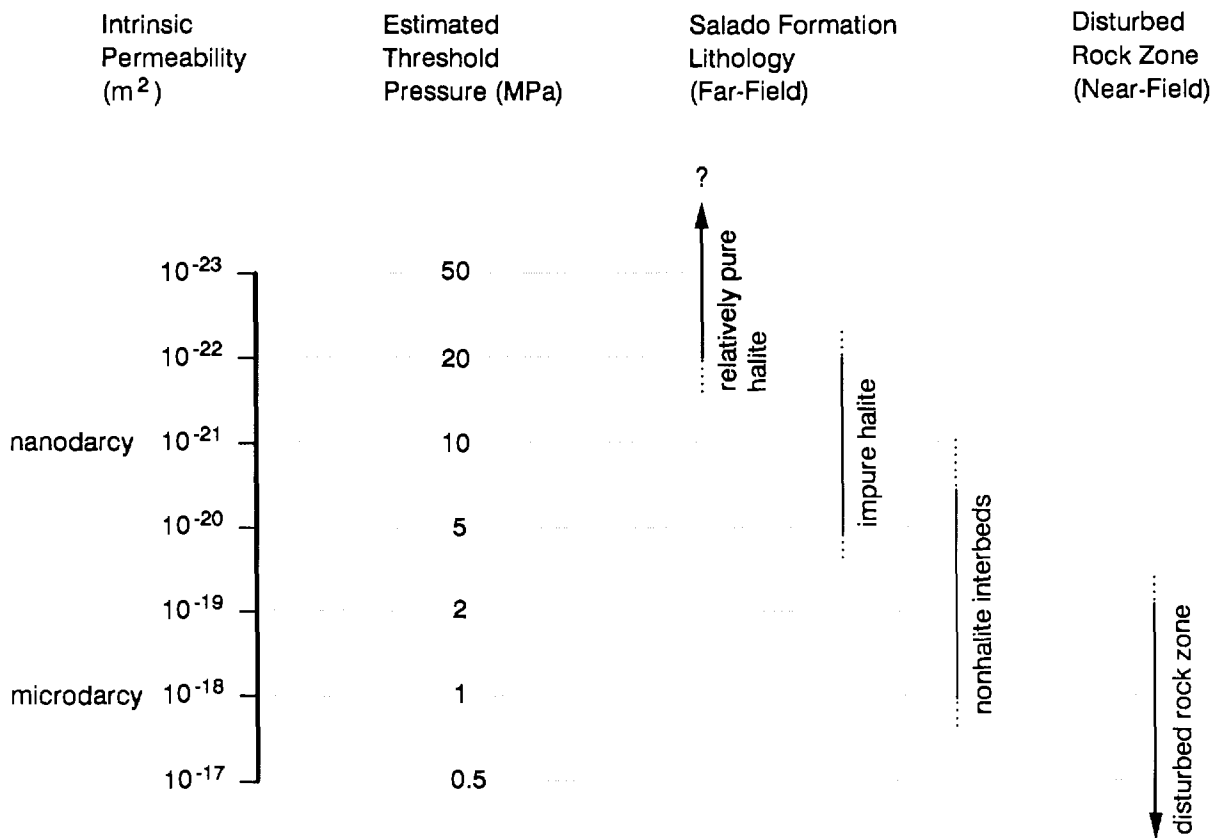
Early underground permeability measurements used gas (nitrogen) injection techniques (Peterson et al., 1985). Complexities in quantifying some of the critical assumptions underlying the interpretation of "gas permeabilities," such as the unknown degree of saturation (Stormont et al., 1987), led to a gradual shift in testing approach to the use of brine-based methods (Peterson et al., 1987; Saulnier and Avis, 1988; Beauheim et al., in review; and Howarth et al., in press). Currently, in situ test activities are focused on permeability measurements in specific stratigraphic units and on the permeability and pore-pressure distribution in the vicinity of a large-scale brine inflow experiment. In addition to measurements designed specifically to determine permeability,

measurements of brine inflow into open observation holes and into controlled experimental holes have also been used to estimate permeability of the surrounding rock (Nowak et al., 1988).

Because both the stratigraphically oriented permeability testing and large-scale brine experiment are ongoing programs, understanding of the permeability distribution in the vicinity of the WIPP disposal rooms is expected to continue to evolve over the next few years. Given the results to date from these ongoing programs and previous permeability measurements, the present understanding of the permeability distribution can be summarized as follows (Figure 9). Permeability within the first two to three meters of an excavation has been increased significantly by near-field deformation effects. Within this zone, permeability is commonly larger than  $10^{-19} \text{ m}^2$  ( $>0.1$  microdarcy) and local fracture zones have significantly larger permeabilities. Relative to far-field gas flow, however, permeability and threshold pressure beyond the disturbed rock zone are of primary interest. Far-field permeability in some of the relatively pure halite units is less than  $10^{-23} \text{ m}^2$  ( $<0.01$  nanodarcy). Permeability in halite units that contain impurities and/or that may have experienced minor amounts of excavation-related deformation is generally in the range from  $10^{-20}$  to  $10^{-22} \text{ m}^2$  (10 to 0.1 nanodarcy). Permeability of Marker Bed 139 and other nonhalite interbeds is highly variable. In some locations, interbed permeability is not significantly different from that of impure halite. In other locations, measured permeabilities of interbeds, most notably in Marker Bed 139, are much higher than that of the halite units. Preliminary results indicate that some interbed permeabilities are as high as  $10^{-18} \text{ m}^2$  (1 microdarcy) (Beauheim et al., in review).

Estimated threshold pressures based on the empirical correlation presented in Equation 11 and Figure 8 are summarized in Figure 9. This empirical correlation suggests that threshold pressures in tight, relatively pure halites are larger than 20 MPa. Threshold pressure in pure halite with permeability less than  $10^{-23} \text{ m}^2$  may be larger than 50 MPa. Threshold pressures in impure halite, halite that may have experienced small amounts of deformation, and relatively tight interbed units are in the range from approximately 5 to 25 MPa. Threshold pressures in more permeable interbed units are in the range from 1 to 2 MPa. Threshold pressure within the disturbed rock zone is likely to be 2 MPa or significantly less.

Threshold pressure estimates based on the empirical correlation presented in Equation 11 have uncertainty associated with the correlation itself and with factors external to the correlation. One uncertainty in the correlation is the error associated with estimating the true mean value of the threshold pressure for a given intrinsic permeability. Because of the relatively strong correlation (goodness-of-fit,  $R^2$ , is equal to 0.93), the estimation error is fairly small (Figure 8). A second uncertainty in the correlation is prediction error due to random variations in threshold pressure in any given rock type and to measurement error in the original data. Because measurement error in the original data was not quantified, these two sources of uncertainty cannot be evaluated independently. The interval between the bounds of this prediction error is approximately three times the estimated mean threshold pressure (Figure 8). One source of uncertainty external to the correlation is the uncertainty associated with measurements of intrinsic permeability in various lithologies of the



TRI-6344-731-0

Figure 9. Plot summarizing estimated threshold pressure for various lithologic units in the Salado Formation based on correlation with intrinsic permeability.

Salado Formation. Beauheim et al. (in review) estimate the uncertainty in their recent Salado permeability measurements to be approximately one half order of magnitude. Uncertainty in the other Salado permeability measurements (Nowak et al., 1988; Howarth et al., in press) has not yet been quantified. Another very important source of uncertainty is the fact that while the data for the correlation span a wide range of consolidated rock types (shale, anhydrite, carbonate, and sandstone), the data do not include any actual measurements from the Salado Formation at the WIPP repository nor do the data include any actual measurements on halite. At this time, it is not possible to quantify the total uncertainty associated with these estimates. Clearly the total uncertainty is quite large and could be reduced significantly by making direct threshold pressure measurements for selected lithologic units of the Salado Formation.

## **5.2 Estimates Based on Capillary Tube Model**

A second approach for estimating threshold pressure in the Salado Formation is to use the capillary tube model expressed in Equation 9. The advantage of this approach is that the capillary tube model provides a more rigorous accounting for the range of physical properties that may influence threshold pressure. One disadvantage of applying this model is that the Salado is a heterogenous formation and values for the complete parameter suite are not currently available for each of the halite and interbed lithologies. Therefore, threshold pressures estimated using the capillary tube model are limited to rough estimates of the gross characteristics of the formation. A second disadvantage of applying this model is that all Salado permeabilities are less than  $10^{-17} \text{m}^2$ , which is the range where the capillary tube model produces somewhat less accurate estimations (Section 4.2 and Figure 7).

Except for formation factor, all of the capillary tube parameters are available for the Salado Formation. An estimate for formation factor can be derived from in situ geophysical measurements. A best estimate of resistivity of the Salado beyond the disturbed rock zone is 120 ohm-meters, which represents the midpoint of the range estimated for 10 to 20 meters out from the excavation using EM-34 electro-magnetic surveys and is within the dominant 100 to 300 ohm-meter range of apparent resistivity measured using DC electric surveys (Skokan et al., 1989). Resistivity of saturated NaCl brine is 0.044 ohm-meter (Asquith, 1982). Using these values, Equation 8 yields a best estimate of average formation factor of  $2.7 \times 10^3$  for the Salado Formation.

Table 4 summarizes best estimates and associated rationales for parameter values describing the gross physical characteristics of the Salado Formation. These best estimates are considered representative of impure halite, which comprises more than 50 percent of the Salado in the immediate vicinity of the repository. Using these values, the estimated threshold pressure based on the capillary tube model is 5 MPa. Given the large range of permeabilities in different lithologies and uncertainty in porosity and formation resistivity factor, this threshold pressure could easily be at least an order of magnitude higher (50 MPa) in stratigraphic units consisting of relatively pure halite and at least an order of magnitude lower (0.5 MPa) in some of the nonhalite interbeds. This 0.5 to 50 MPa range is similar to the range estimated using the intrinsic-permeability correlation.

**Table 4. Parameter values for estimating threshold pressure of the Salado Formation (far-field) based on the capillary tube model.**

PARAMETER	ESTIMATED VALUE	UNITS	RATIONALE	REFERENCE
<b>SURFACE TENSION</b>				
Best estimate	0.07	N/m	Water in contact with air at 20 deg. C	1
Maximum	0.08	N/m	Increase due to dissolved NaCl in saturated brine	1
Minimum	0.05	N/m	Increased pressure (15 MPa), natural gas in water	2
<b>PORE SHAPE FACTOR</b>				
Best estimate	3	-	Shape factor value for high aspect ratio pore space	3
Maximum	3	-	Shape factor value for high aspect ratio pore space	3
Minimum	2	-	Shape factor value for circular pores	3
<b>FORMATION FACTOR</b>				
Best estimate	$2.7 \times 10^3$	-	Midpoint of EM-34 range, in max. cluster DC meas.	4
Maximum	$2.5 \times 10^4$	-	High end of DC measurement resistivity range	4
Minimum	$2.5 \times 10^2$	-	Low end of DC measurement resistivity range	4
<b>POROSITY</b>				
Best estimate	0.01	-	Best estimate, weight loss from heating	5
Maximum	0.05	-	High end of range from EM and resistivity meas.	4
Minimum	0.001	-	Low end of range from drying data	6
<b>PERMEABILITY</b>				
Best estimate	$10^{-21}$	$m^2$	Midpoint of range for impure halite	7, 8
Maximum	$10^{-18}$	$m^2$	Approx. high end of range for thin interbed zones	7
Minimum	$<10^{-23}$	$m^2$	Approx. low end of range for relatively pure halite	7, 8

- References: 1 Weast, 1978  
2 Hocott, 1939  
3 Wyllie and Spangler, 1952  
4 Skokan et al., 1989  
5 Black et al., 1983  
6 Powers et al., 1978  
7 Beauheim et al., in review  
8 Howarth et al., in press

## **6. OTHER PROCESSES AND PHYSICAL CHARACTERISTICS THAT MAY INFLUENCE THRESHOLD PRESSURE IN THE WIPP ENVIRONMENT**

The preceding discussions focus on threshold pressure in fully saturated, porous media. Other processes and physical characteristics that occur in the WIPP environment may have an impact on threshold pressure. Potentially important processes include partial desaturation and fracturing of rock adjacent to the excavations. A potentially important physical characteristic is the possibility that undeformed, relatively pure halite (i.e., relatively pure halite units located beyond the near-field zone experiencing excavation-related deformation) actually has zero permeability.

### **6.1 Threshold Pressure Under Partially Saturated Conditions**

A combination of geophysical measurements and gas-injection tests suggests that some portion of the rock in the immediate vicinity (i.e. first few meters) of the WIPP excavations may be partially saturated (Stormont et al., 1987; Borns and Stormont, 1988). Processes that may contribute to desaturating rock near the excavations include dilatation, drying, and exsolution of dissolved gas present in Salado brine.

Dilatation is an increase in the size of existing pores or the creation of new pore space by opening along grain boundaries and/or microfracturing that occurs in response to the strongly modified stress field adjacent to an excavation (Jaeger and Cook, 1976; Golder Associates, Inc., 1987). The drop in fluid pressure associated with increased pore volume may draw air into the pores (near the surface of the excavation) and/or may cause dissolved gas in the pore fluid to come out of solution. In either case, an important by-product of dilatation may be the creation of partially saturated pores.

Drying in a porous medium initially occurs as vaporization at the surface of the medium in contact with unsaturated air (McCabe et al., 1985). As water at the surface is depleted, water from the interior is drawn to the surface by capillary forces in the smaller pores, while larger pores in the interior are drained and air enters to replace the displaced water. Once the larger pores are drained, capillary forces in the smaller pores become large enough to move the primary drying surface into the interior of the medium. In a fractured porous medium, early drainage of relatively large aperture fractures may effectively extend active drying surfaces into the interior of the medium, thereby enhancing the overall drying process.

The exsolution of dissolved gas (primarily nitrogen) that occurs naturally in the Salado brine is a third process that may contribute to the creation of partially saturated conditions. In the WIPP mine, the presence of gas is manifested in several ways: 1) gas is observed exsolving in brine weeps on some walls of the excavation; 2) gas is present in many brine samples; 3) gas bubbles are observed in some of the brine observation holes; 4) gas has been encountered in some pressurized test intervals within the Salado; and 5) gas is present in fluid inclusions within individual halite crystals (Peterson et al., 1985; Stein and Krumhansl, 1986; Deal and Case, 1987; Beauheim et al., in review). These

observations indicate that brine from the Salado Formation contains dissolved gas that comes out of solution as fluid pressure is decreased. If gas exsolution is occurring within the Salado, an important by-product of this process is its contribution to decreasing the degree of water saturation in the near field. An important unknown at the present time is the amount of gas present under undisturbed conditions. At one extreme, Salado brine may be fully gas saturated with free gas present at undisturbed pore pressures. At the other extreme, Salado brine may contain only a small quantity of dissolved gas, which comes out of solution only at pressures near atmospheric. The amount of gas in solution will strongly influence how far from the excavations desaturation is occurring due to gas exsolution.

The effect of desaturation on threshold pressure was first studied by Hassler et al. (1943) in the context of oil reservoirs in which production is driven in part by gas exsolution at levels that are insufficient to cause the development of an interconnected gas-filled pore network. This work was later extended to gas-reservoir caprock environments by Thomas et al. (1968) in the context of resealing caprocks once the initial threshold pressure has been exceeded. This research indicates that the impact of desaturation is to reduce threshold pressures progressively until the critical gas saturation is reached, corresponding to the incipient formation of an interconnected, gas-filled pore network (Figure 3). Crossing this critical gas saturation threshold is associated with the initial development of nonzero gas relative permeabilities. At water saturations below the critical gas saturation, threshold pressure is zero. Therefore, the processes of dilatation, drying, and exsolution of dissolved gas from the Salado brine are likely to significantly reduce threshold pressures in the immediate vicinity of the WIPP excavations. These conditions will enhance the ability of waste-generated gas to penetrate and flow through the disturbed rock zone, providing enhanced gas pathways between the room and the higher permeability, nonhalite interbeds. These conditions may also reduce threshold pressure in the halite units of the disturbed rock zone to a level that allows gas penetration into the halite.

## **6.2 Impact of Fracturing on Threshold Pressure**

In low-permeability environments, the presence of fractures frequently dominates hydraulic behavior. In a tight porous material containing small intergranular pores, the existence or introduction of fractures is likely to provide pore space with much larger apertures. The presence of such large-aperture pore space causes a significant reduction in threshold pressure of the total rock mass. Indeed, the presence of natural or induced fractures is considered one of the most important elements in the evaluation of potential caprocks for underground gas storage reservoirs, as the presence of fractures can produce significant leaks (Ibrahim et al., 1970; Katz and Coates, 1973).

Two types of fracturing occur in the vicinity of the WIPP excavations. The first type of fracturing is caused by the redistribution of stress in the immediate vicinity of the excavation. The second type of fracturing is natural, pre-excavation fractures in the relatively brittle anhydrite of Marker Bed 139 and other anhydrite interbeds.

Excavation-related fracturing has been documented by visual observations in holes drilled from the excavations, by geophysical measurements, and by gas injection (Borns and Stormont, 1988; U.S. DOE, 1988). This fracturing includes vertical separations along nonhalite interbeds in the floor and back, arcuate fractures in the floor and back that crosscut a variety of stratigraphic units, and vertical fractures associated with spalling within the ribs. The intensity and extent of fracturing are a function of time and of excavation dimensions. Gas-injection measurements indicate that in the vicinity of a typical drift that has been open for several years, fracturing is most extensive within the first two meters of the excavation (Stormont et al., 1987; Borns and Stormont, 1988). During these tests, gas flow into this zone occurred at test-zone pressures of less than 1 MPa.

In a study of large-diameter drill core, Borns (1985) documented the presence of horizontal and low-angle fractures within Marker Bed 139 that predate the WIPP excavations. While these fractures are much more subtle than those related to the excavation stresses, they are only partially healed and may play an important role in controlling far-field permeability of anhydrite interbeds and the overall hydrologic response of the Salado Formation to the WIPP facility. Borns (1985) concluded that these fractures formed in response to stress cycles related to sedimentation and erosion or in response to deformation in the underlying Castile Formation. In either case, other relatively brittle anhydrite and polyhalite interbeds within the Salado probably responded in a similar fashion. Therefore, it is likely that similar fractures exist in other interbeds as well.

The presence of extensive, excavation-related fracturing adjacent to the WIPP repository will most likely create pore space that is available for the storage of waste-generated gas. In the context of the total room/rock system, this pore space does not actually represent new void volume, but rather represents a redistribution of void volume from the room to the disturbed rock zone. Given the relatively large apertures and corresponding low threshold pressure of fractures, this pore space should be readily accessible to gas that is generated in the adjacent room and will significantly enhance gas flow between the room and the relatively high permeability, nonhalite interbeds. Beyond this zone, the presence of naturally occurring, partially healed fractures in Marker Bed 139 and other similar interbeds may provide potential gas flow pathways that have threshold pressures significantly lower than the 0.5 to 5 MPa range estimated based on empirical correlation with permeability and on the capillary tube model (Section 5).

### **6.3 Possibility of Zero Permeability in Undeformed, Pure Halite**

Because of halite's plastic deformation behavior and low yield strength, it is theoretically not possible to maintain open, interconnected pore space, leading to the general conclusion that halite is impermeable (National Academy of Sciences, 1957). Based on this type of reasoning and on field observations of the occurrence and character of fluids encountered during the mining of salt deposits in Europe, Baar (1977) drew the conclusion that salt deposits are absolutely impermeable at depths of 300 meters or more. Similar conclusions were drawn relative to the Salado Formation during the early stages of the WIPP project (Powers et al., 1978).

Experimental confirmation of absolute zero permeability is not possible. Both laboratory and in situ permeability measurements always have some lower limit of resolution due to equipment limitations. As permeability measurement techniques have been refined and lower limits of resolution achieved, tight rock that was once considered impermeable has been shown to have measurable permeability and measurable heterogeneity at levels below earlier limits of resolution.

Technical arguments concerning the absolute impermeability of halite based on its mechanical behavior rigorously apply only to pure halite. The presence of significant impurities can alter the deformation behavior of halite and absolute impermeability is less likely. Going one step further, continuous interbeds of nonhalite material such as clay or anhydrite may be layers that contain interconnected pore space, which provide thin, low-permeability pathways imbedded within a much larger mass of very low permeability and/or truly impermeable material.

Recent in situ permeability testing in the Salado Formation has encountered a number of relatively pure halite units that maintain large and arbitrary pressures within a test interval for an extended period of time with no observable pressure decay (Beauheim et al., in review; Howarth et al., in press). These units are currently considered to have a permeability of less than approximately  $10^{-23} \text{ m}^2$ . At present, it is not possible to determine whether or not these units have a finite permeability (e.g.,  $10^{-24} \text{ m}^2$ ) or whether permeability is absolutely zero. Therefore, one must consider the permeability question in the context of a specific problem, which in this case is the penetration and flow of gas under repository conditions. Threshold pressures are likely to be so high in such a tight material that relative permeability to gas of these tight, pure, undeformed halite units is absolutely zero for the range of pressure conditions that are possible in the repository environment.

## 7. DISCUSSION

Anoxic corrosion and microbial degradation of the WIPP waste may produce sufficient quantities of gas to generate high pressure in the repository. An important objective in assessing the impact of waste-generated gas is evaluating whether or not gas can flow into the surrounding rock, thereby moderating gas pressure. If gas can flow outward, then understanding and quantifying the processes by which this occurs is also very important. If the surrounding rock is fully saturated with brine, then the relative permeability to gas is zero and no gas can flow can occur. In order for gas to flow from a waste repository into the surrounding rock, it must first overcome the sum of the capillary forces resisting penetration (threshold pressure) and the existing brine pressure in the rock pores, and then establish interconnected gas pathways (corresponding to a nonzero relative permeability to gas) that allow outward flow. Threshold pressure is controlled primarily by pore size and pore interconnections. Because pore space in the bedded salt surrounding the WIPP repository is characterized by extremely small apertures, threshold pressures may be quite large. The primary objectives of this study have been to estimate the magnitude of threshold pressure in the bedded salt formation that surrounds the WIPP repository and to evaluate the role that this parameter may play in controlling the outward flow of waste-generated gas.

### 7.1 Threshold Pressure Estimates for the Salado Formation

Estimates of threshold pressure for the Salado Formation have been made based on an empirical correlation of threshold pressure with intrinsic permeability and on a capillary tube model. The physical rationale behind the correlation approach is that both threshold pressure and intrinsic permeability are controlled, to a large degree, by pore size and pore interconnections. Data for this correlation come primarily from laboratory measurements of threshold pressure and intrinsic permeability on low-permeability caprock materials associated with underground gas-storage studies and on other consolidated rock types. The capillary tube model also comes from underground gas-storage technology and is derived from an idealized capillary tube representation of a porous medium. The permeability correlation and capillary tube model yield generally consistent estimates of threshold pressures for the Salado Formation at the WIPP. These estimates indicate that threshold pressures in relatively pure, undeformed halite may be 20 to 50 MPa, or larger. Threshold pressure of impure halite, mildly deformed halite, and some interbeds is estimated to be on the order of 5 to 25 MPa. Other interbed units, in particular those containing preexisting, partially healed fractures, are estimated to have threshold pressures on the order of 2 to 1/2 MPa, or less. *Because of the compounding effect of low threshold pressure and relatively high intrinsic permeability, these nonhalite interbeds are likely to be the dominant pathways for flow of waste-generated gas away from a pressurized repository.*

The potential importance of nonhalite interbeds can be viewed from a second perspective. If one assumes that the Salado Formation is fully saturated with brine at 12 MPa in the far field and that gas pressure should not exceed lithostatic pressure (15 MPa), then in this far-field region, only lithologic units with a threshold pressure of less than 3 MPa are capable of allowing gas penetration

and the development of interconnected gas-flow paths without exceeding the 15 MPa pressure criteria. Based on estimated threshold pressures for the various Salado lithologies, only the more permeable, nonhalite interbeds are likely to meet this criteria. It should be noted, however, that the lower end of the estimated threshold pressure range for impure halite is 5 MPa, which is close to the 3 MPa criteria for far-field gas penetration and flow. Given the large uncertainties associated with the estimated threshold pressures, it is quite possible that actual threshold pressure in the impure halite of the Salado is less than 3 MPa. This possibility is potentially important because impure halite comprises more than 50 percent of the Salado Formation in the vicinity of the repository and, therefore, represents a significant potential for gas storage.

The discussion thus far has focused primarily on the role of threshold pressure under far-field conditions. Near the repository, a number of processes occur that may significantly reduce threshold pressure. Local fracturing and pore dilatation in response to excavation-related stresses create larger pore apertures (Section 6.2). Desaturation occurs as a result of drying, dilatation, and/or exsolution of gas dissolved in Salado brine under natural conditions (Section 6.1). All of these processes contribute to the development of a zone surrounding the repository that contains pore space that will be readily accessible to waste-generated gas due to significantly decreased threshold pressures. The ready accessibility of the near-field region to gas flow has already been demonstrated at the WIPP by the successful injection of gas in near-field test zones at test zone pressures of less than 1 MPa (Section 6.2). This zone is likely to provide partially desaturated pathways for gas flow from the disposal rooms to nearby nonhalite interbeds that have relatively high permeabilities and low threshold pressures. This near-field zone may also contain significant gas storage potential.

While the threshold pressure estimates discussed in this report are quite useful for formulating concepts and constructing preliminary models of system behavior, the reader is cautioned that there remains considerable uncertainty in these estimates. *These estimates and analyses are based on threshold pressure information from nonsalt rock types and must be confirmed with in situ or laboratory measurements that are specific to the Salado Formation at the WIPP repository.* In particular, such measurements should be directed toward two lithologies, nonhalite interbeds and impure halite. The nonhalite interbeds are the most likely units to have the combination of low threshold pressure and sufficient permeability to allow significant gas flow laterally away from the repository. Because some of the interbed units contain partially healed, pre-existing fractures, laboratory testing may require unusually large samples and in situ testing may be necessary. If threshold pressure in the impure halite is low enough, then these units may provide a relatively large gas-storage volume. Therefore, a second target for WIPP-specific threshold pressure measurements should be impure halite.

## **7.2 Conceptual Model for Hydrologic Response of the Repository to Waste-Generated Gas**

The threshold pressure estimates and related analyses discussed in this report indicate that threshold pressure is likely to be a very important parameter controlling the flow of waste-generated gas from the WIPP repository into the adjacent Salado Formation. Threshold pressure may allow gas penetration and flow along thin, nonhalite interbeds and at the same time prevent significant gas penetration into the halite, which makes up much of the Salado Formation. A conceptual model for the overall system that incorporates this behavior can be summarized as follows. During the early post-closure time period, waste-generated gas (at relatively low pressure) accumulates and is confined to the available pore space within a disposal room and perhaps a thin zone of fractured, depressurized, and partially desaturated rock adjacent to the disposal room. Confinement within this area is provided by a combination of low permeability, moderate to high threshold pressure, and moderate to high pore-fluid pressures in the surrounding rock. However, the surrounding rock is not homogeneous. Heterogeneities in the form of thin, nonhalite interbeds are likely to be a very important factor. In contrast to the high threshold pressure in halite, threshold pressure in the nonhalite interbeds is likely to be low enough for gas to readily penetrate and flow laterally along these units. Also, because of the higher intrinsic permeability of these interbeds, depressurization due to brine drainage is likely to be more extensive than in the halite. Given the combined effects of lower threshold pressure, lower pore fluid pressure, and higher intrinsic permeability, these nonhalite interbeds will be the dominant pathways for flow of waste-generated gas away from the pressurized repository and outward gas flow along the interbeds is likely to be initiated at room pressures well below lithostatic. Gas-flow pathways between the repository and nonhalite interbeds will be provided by the disturbed rock zone and by vertical boreholes (3 to 15 meters in length) drilled for rock bolting and other geotechnical purposes.

The next important step in assessing the impact of waste-generated gas on the WIPP repository is quantifying and testing the conceptual model presented in the previous paragraph. This requires the iterative development of numerical models for assessing system behavior and experimental work to provide data on pertinent physical parameters and processes. Analyses to date indicate strong coupling between the chemical processes controlling gas-generation rates, fluid processes controlling brine flow to disposal rooms and gas flow away from disposal rooms, and mechanical processes controlling room closure and the amount of void space available for gas storage. Assessing the chemical, hydrologic, and mechanical responses the WIPP repository to rising gas pressure is the focus of ongoing modeling and experimental studies at Sandia.



## 8. REFERENCES

- Asquith, G.B. 1982. *Basic Well Log Analysis for Geologists*. Tulsa, Oklahoma: American Association of Petroleum Geologists.
- Baar, C.A. 1977. *Applied Salt-Rock Mechanics*. Amsterdam: Elsevier Scientific Publishing Company.
- Barker, J.A., and S.S.D. Foster. 1981. "A Diffusion Exchange Model for Solute Movement in Fissured Porous Rock." *Quarterly Journal of Engineering Geology* vol. 14.
- Bear, J. 1972. *Dynamics of Fluids in Porous Media*. New York: American Elsevier Publishing Company, Inc.
- Beauheim, R.L. 1986. *Hydraulic-Test Interpretations for Well DOE-2 at the Waste Isolation Pilot Plant (WIPP) Site*. SAND86-1364. Albuquerque, New Mexico: Sandia National Laboratories.
- Beauheim, R.L., G.J. Saulnier, and J.D. Avis. (in review). *Interpretation of Brine-Permeability Tests of the Salado Formation at the Waste Isolation Pilot Plant*. SAND90-0083. Albuquerque, New Mexico: Sandia National Laboratories.
- Black, S.R., R.S. Newton, and D.K. Shukla. 1983. *Results of Site Validation Experiments, Waste Isolation Pilot Plant (WIPP) Project, Southeastern New Mexico*. TME 3177. Albuquerque, New Mexico: U.S. Department of Energy.
- Borns, D.J. 1985. *Marker Bed 139: A Study of Drillcore from a Systematic Array*. SAND85-0023. Albuquerque, New Mexico: Sandia National Laboratories.
- Borns, D.J., and J.C. Stormont. 1988. *An Interim Report on Excavation Effect Studies at the Waste Isolation Pilot Plant: The Delineation of the Disturbed Rock Zone*. SAND87-1375. Albuquerque, New Mexico: Sandia National Laboratories.
- Borns, D.J., and J.C. Stormont. 1989. "The Delineation of the Disturbed Rock Zone Surrounding Excavations in Salt" in *Proceedings of the 30th U.S. Rock Mechanics Symposia at the University of West Virginia, June 19-22, 1989*. Rotterdam, Netherlands: A.A. Balkeema.
- Brooks, R.H., and A.T. Corey. 1964. *Hydraulic Properties of Porous Media*. Colorado State University, Hydrology Paper No. 3.
- Brush, L.H. 1990. *Test Plan for Laboratory and Modeling Studies of Repository and Radionuclide Chemistry for the Waste Isolation Pilot Plant*. SAND90-0266. Albuquerque, New Mexico: Sandia National Laboratories.
- Calhoun, J.C. 1953. *Fundamentals of Reservoir Engineering*. Norman, Oklahoma: University of Oklahoma Press.

- Carden, P.O., and L. Paterson. 1979. "Physical, Chemical and Energy Aspects of Underground Hydrogen Storage." *International Journal of Hydrogen Energy* vol. 4: 559-569.
- Cosby, B.J., G.M. Hornberger, R.B. Clapp, and T.R. Ginn. 1984. "A Statistical Exploration of the Relationships of Soil Moisture Characteristics to the Physical Properties of Soils." *Water Resources Research* vol. 20, no. 6: 682-690.
- Deal, D.E., and J.B. Case. 1987. *Brine Sampling and Evaluation Program Phase I Report*. DOE/WIPP 87-008. Carlsbad, New Mexico: U.S. Department of Energy, WIPP Project Office.
- de Marsily, G. 1986. *Quantitative Hydrology*. Orlando, Florida: Academic Press.
- Dullien, F.A.L. 1979. *Porous Media, Fluid Transport and Pore Structure*. New York: Academic Press.
- Freeze, R.A., and J.A. Cherry. 1979. *Groundwater*. Englewood Cliffs, New Jersey: Prentice-Hall.
- Golder Associates, Inc. 1987. *Assessment of the Character and Extent of Mechanical Disturbance for Underground Openings in Salt*. BMI/ONWI/C-1. Columbus, Ohio: Office of Nuclear Waste Isolation, Battelle Memorial Institute.
- Hassler, G.L., E. Brunner, and T.J. Deahl. 1943. "The Role of Capillarity in Oil Production." *Petroleum Technology* vol. 155: 155-174.
- Hocott, C.R. 1939. "Interfacial Tension Between Water and Oil Under Reservoir Conditions." *Transactions of the American Association of Mining and Metallurgical Engineers* vol. 132: 184-190.
- Howarth, S.M., E.W. Peterson, P.L. Lagus, K. Lie, S.J. Finley, and J.E. Nowak. (in press). "Interpretation of In-Situ Pressure and Flow Measurements of the Salado Formation at the Waste Isolation Pilot Plant." *Society of Petroleum Engineers*, Paper #21840.
- Hubbert, M.K. 1953. "Entrapment of Petroleum Under Hydrodynamic Conditions." *Association of Petroleum Geologists Bulletin* vol. 37, no. 8: 1954-2026.
- Ibrahim, M.A., M.R. Tek, and D.L. Katz. 1970. *Threshold Pressure in Gas Storage*. Arlington, Virginia: American Gas Association, Inc.
- Jaeger, J.C., and N.G.W. Cook. 1976. *Fundamentals of Rock Mechanics*. London: Chapman and Hall.
- Katz, D.L., and K.H. Coats. 1973. *Underground Storage of Fluids*. Ann Arbor, Michigan: Ulrich's Books, Inc.
- Katz, D.L., and E.R. Lady. 1976. *Compressed Air Storage for Electric Power Generation*. Ann Arbor, Michigan: Ulrich's Books, Inc.

- Katz, D.L., and M.R. Tek. 1970. "Storage of Natural Gas in Saline Aquifers." *Water Resources Research* vol. 6, no. 5: 1515-1521.
- Katz, D.L., D. Cornell, R. Kobayashi, F.H. Poettmann, J.A. Vary, J.R. Elenbaas, and C.F. Weinaug. 1959. *Handbook of Natural Gas Engineering*. New York: McGraw-Hill Book Company.
- Lappin A.R., R.L. Hunter, D.P. Garber, and P.B. Davies. 1989. *Systems Analysis, Long-Term Radionuclide Transport, and Dose Assessments, Waste Isolation Pilot Plant (WIPP), Southeastern New Mexico; March 1989*. SAND89-0462. Albuquerque, New Mexico: Sandia National Laboratories.
- McCabe, W.L., J.C. Smith, and P. Harriott. 1985. *Unit Operations of Chemical Engineering*. New York: McGraw-Hill Book Company.
- McTigue, D.F., S.J. Finley, and E.J. Nowak. 1989. "Brine Transport in Polycrystalline Salt - Field Measurements and Model Considerations." *Transactions, American Geophysical Union* vol. 70, no. 43: 1111.
- Muskat, M. 1949. *Physical Principles of Oil Production*. New York: McGraw-Hill Book Company, Inc.
- National Academy of Sciences. 1957. *The Disposal of Radioactive Waste on Land*. Publication 519. Washington, D.C.: National Academy of Sciences, National Research Council.
- Nowak, E.J., and D.F. McTigue. 1987. *Interim Results of Brine Transport Studies in the Waste Isolation Pilot Plant (WIPP)*. SAND87-0880. Albuquerque, New Mexico: Sandia National Laboratories.
- Nowak, E.J., D.F. McTigue, and R. Beraun. 1988. *Brine Inflow to WIPP Disposal Rooms: Data, Modeling, and Assessment*. SAND88-0112. Albuquerque, New Mexico: Sandia National Laboratories.
- Pandey, G.N., M.R. Tek, and D.L. Katz. 1973. "Studies of Front-End Threshold Pressure Measurements." *American Gas Association Transmission Conference*. T112-T116.
- Peterson, E., P. Lagus, J. Brown, and K. Lie. 1985. *WIPP Horizon In Situ Permeability Measurements Final Report*. SAND85-7166. Albuquerque, New Mexico: Sandia National Laboratories.
- Peterson, E.W., P.L. Lagus, and K. Lie. 1987. *WIPP Horizon Free Field Fluid Transport Characteristics*. SAND87-7164. Albuquerque, New Mexico: Sandia National Laboratories.
- Powers, D.W., S.J. Lambert, S.E. Shaffer, L.R. Hill, and W.D. Weart, eds. 1978. *Geological Characterization Report, Waste Isolation Pilot Plant (WIPP) Site, Southeastern New Mexico*. SAND78-1596. Albuquerque, New Mexico: Sandia National Laboratories.

- Purcell, W.R. 1949. "Capillary Pressures--Their Measurements Using Mercury and the Calculation of Permeability Therefrom." *Transactions of the American Institute of Mining and Metallurgical Engineers* vol. 186: 39-48.
- Rose, W., and W.A. Bruce. 1949. "Evaluation of Capillary Character in Petroleum Reservoir Rock." *Transactions of the American Institute of Mining and Metallurgical Engineers* vol. 186: 127-142.
- Saito, H. 1963. "Capillary Pressure Measurements of Porous Medium by Vapor Pressure Method." in *Sixth World Petroleum Congress, Frankfurt, Germany, June, 1963*. 155-162.
- Saulnier, G.J., and J.D. Avis. 1988. *Interpretation of Hydraulic Tests Conducted in the Waste-Handling Shaft at the Waste Isolation Pilot Plant (WIPP) Site*. SAND88-7001. Albuquerque, New Mexico: Sandia National Laboratories.
- Skokan, C.K., M.C. Pfeifer, G.V. Keller, and H.T. Anderson. 1989. *Studies of Electrical and Electromagnetic Methods for Characterizing Salt Properties at the WIPP Site, New Mexico*. SAND87-7174. Albuquerque, New Mexico: Sandia National Laboratories.
- Stakman, W.P. 1968. "The Relation Between Particle Size, Pore Size and Hydraulic Conductivity of Sand Separates." *International Association of Hydrologic Sciences, Publication No. 82*. 373-383.
- Stein, C.L., and J.L. Krumhansl. 1986. *Chemistry of Brines from the Waste Isolation Pilot Plant (WIPP), Southeastern New Mexico*. SAND85-0897. Albuquerque, New Mexico: Sandia National Laboratories.
- Stormont, J.C., E.W. Peterson, and P.L. Lagus. 1987. *Summary of and Observations About WIPP Facility Horizon Flow Measurements Through 1986*. SAND87-0176. Albuquerque, New Mexico: Sandia National Laboratories.
- Thomas, L.K., D.L. Katz, and M.R. Tek. 1968. "Threshold Pressure Phenomena in Porous Media." *Society of Petroleum Engineers Journal* vol. 8, no. 2: 174-184.
- U.S. Department of Energy. 1988. *Geotechnical Field Data and Analysis Report: June 1986 - June 1987*. DOE/WIPP 87-017. Carlsbad, New Mexico: U.S. Department of Energy, WIPP Project Office.
- Weast, R.C. 1978. *CRC Handbook of Chemistry and Physics*. West Palm Beach, Florida: CRC Press.
- Wyllie, M.R.J., and W.D. Rose. 1950. "Some Theoretical Considerations Related to the Quantitative Evaluation of the Physical Characteristics of Reservoir Rock from Electric Log Data." *Transactions of the American Institute of Mining and Metallurgical Engineers* vol. 189: 105-118.

Wyllie, M.R.J., and M.B. Spangler. 1952. "Application of Electrical Resistivity Measurements to Problem of Fluid Flow in Porous Media." *American Association of Petroleum Geologists Bulletin* vol. 36, no. 2: 359-403.



FEDERAL AGENCIES

U. S. Department of Energy, (5)  
Office of Civilian Radioactive  
Waste Management

Attn: Deputy Director, RW-2  
Associate Director, RW-10  
Office of Program Administration  
and Resources Management  
Associate Director, RW-20  
Office of Facilities Siting  
and Development  
Associate Director, RW-30  
Office of Systems Integration  
and Regulations  
Associate Director, RW-40  
Office of External Relations  
and Policy  
Forrestal Building  
Washington, DC 20585

U. S. Department of Energy (3)  
Albuquerque Operations Office  
Attn: J. E. Bickel  
R. Marquez, Director  
Public Affairs Division  
P.O. Box 5400  
Albuquerque, NM 87185

U.S. Department of Energy  
Attn: National Atomic Museum Library  
Albuquerque Operations Office  
P.O. Box 5400  
Albuquerque, NM 87185

U.S. Department of Energy (5)  
WIPP Project Office (Carlsbad)  
Attn: Vernon Daub  
J. A. Mewhinney  
J. Carr  
P.O. Box 3090  
Carlsbad, NM 88221

U.S. Department of Energy  
Research and Waste Management Division  
Attn: Director  
P.O. Box E  
Oak Ridge, TN 37831

U.S. Department of Energy  
Waste Management Division  
Attn: R. F. Guercia  
P.O. Box 550  
Richland, WA 99352

U.S. Department of Energy (1)  
Attn: Edward Young  
Room E-178  
GAO/RCED/GTN  
Washington, DC 20545

U.S. Department of Energy (6)  
Office of Environmental Restoration  
and Waste Management  
Attn: Jill Lytle, EM30  
Mark Frei, EM-34 (3)  
Mark Duff, EM-34  
Clyde Frank, EM-50  
Washington, DC 20585

U.S. Department of Energy (3)  
Office of Environment, Safety  
and Health  
Attn: Ray Pelletier, EH-231  
Kathleen Taimi, EH-232  
Carol Borgstrom, EH-25  
Washington, DC 20585

U.S. Department of Energy (2)  
Idaho Operations Office  
Fuel Processing and Waste  
Management Division  
785 DOE Place  
Idaho Falls, ID 83402

U.S. Department of Energy  
Savannah River Operations Office  
Defense Waste Processing  
Facility Project Office  
Attn: W. D. Pearson  
P.O. Box A  
Aiken, SC 29802

U.S. Environmental Protection Agency (2)  
Attn: Ray Clark  
Office of Radiation Programs (ANR-460)  
Washington, DC 20460

U.S. Geological Survey  
Branch of Regional Geology  
Attn: R. Snyder  
MS913, Box 25046  
Denver Federal Center  
Denver, CO 80225

U.S. Geological Survey  
Conservation Division  
Attn: W. Melton  
P.O. Box 1857  
Roswell, NM 88201

U.S. Geological Survey (2)  
Water Resources Division  
Attn: Russell Livingston  
Suite 200  
4501 Indian School NE  
Albuquerque, NM 87110

U.S. Nuclear Regulatory Commission (4)  
Attn: Joseph Bunting, HLEN 4H3 OWFN  
Ron Ballard, HLGP 4H3 OWFN  
Jacob Philip  
NRC Library  
Mail Stop 623SS  
Washington, DC 20555

#### BOARDS

Defense Nuclear Facilities Safety Board  
Attn: Dermont Winters  
Suite 700  
625 Indiana Ave., NW  
Washington, DC 20004

U.S. Department of Energy  
Advisory Committee on Nuclear  
Facility Safety  
Attn: Meritt E. Langston, AC21  
Washington, DC 20585

Nuclear Waste Technical  
Review Board (2)  
Attn: Dr. Don A. Deere  
Dr. Sidney J. S. Parry  
Suite 910  
1100 Wilson Blvd.  
Arlington, VA 22209-2297

Richard Major  
Advisory Committee  
on Nuclear Waste  
Nuclear Regulatory Commission  
7920 Norfolk Avenue  
Bethesda, MD 20814

#### STATE AGENCIES

Environmental Evaluation Group (3)  
Attn: Library  
Suite F-2  
7007 Wyoming Blvd., NE  
Albuquerque, NM 87109

New Mexico Bureau of Mines  
and Mineral Resources (2)  
Attn: F. E. Kottolowksi, Director  
J. Hawley  
Socorro, NM 87801

NM Department of Energy & Minerals  
Attn: Librarian  
2040 S. Pacheco  
Santa Fe, NM 87505

NM Environmental Improvement Division  
Attn: Deputy Director  
1190 St. Francis Drive  
Santa Fe, NM 87503

#### LABORATORIES/CORPORATIONS

Battelle Pacific Northwest Laboratories (5)  
Attn: D. J. Bradley, K6-24  
J. Relyea, H4-54  
R. E. Westerman, P8-37  
H. C. Burkholder, P7-41  
L. Pederson, K6-47  
Battelle Blvd.  
Richland, WA 99352

Savannah River Laboratory (6)  
Attn: N. Bibler  
E. L. Albenisius  
M. J. Plodinec  
G. G. Wicks  
C. Jantzen  
J. A. Stone  
Aiken, SC 29801

George Dymmel  
SAIC  
101 Convention Center Dr.  
Las Vegas, NV 89109

INTERA Inc. (5)  
Attn: J. F. Pickens  
G. A. Freeze  
M. Reeves  
R. F. Jackson  
Suite #300  
6850 Austin Center Blvd.  
Austin, TX 78731

INTERA Inc.  
Attn: Wayne Stensrud  
P.O. Box 2123  
Carlsbad, NM 88221

IT Corporation (2)  
Attn: R. F. McKinney  
J. Myers  
Regional Office - Suite 700  
5301 Central Avenue, NE  
Albuquerque, NM 87108

IT Corporation (2)  
Attn: D. E. Deal  
P.O. Box 2078  
Carlsbad, NM 88221

Charles R. Hadlock  
Arthur D. Little, Inc.  
Acorn Park  
Cambridge, MA 02140-2390

Lawrence Berkeley Laboratory  
Earth Sciences Division (4)  
Attn: J. Long  
S. Martel  
K. Pruess  
C. F. Tsang  
1 Cyclotron Road  
Berkeley, CA 94720

Los Alamos National Laboratory  
Attn: B. Erdal, CNC-11  
P.O. Box 1663  
Los Alamos, NM 87544

RE/SPEC, Inc. (2)  
Attn: W. Coons  
P. F. Gnirk  
Suite 300  
4775 Indian School Rd., NE  
Albuquerque, NM 87110-3927

RE/SPEC, Inc. (7)  
Attn: L. L. Van Sambeek  
G. Callahan  
T. Pfeifle  
J. L. Ratigan  
P.O. Box 725  
Rapid City, SD 57709

Center for Nuclear Waste  
Regulatory Analysis (4)  
Attn: P. K. Nair  
Southwest Research Institute  
6220 Culebra Road  
San Antonio, TX 78228-0510

Science Applications  
International Corporation  
Attn: Howard R. Pratt,  
Senior Vice President  
10260 Campus Point Drive  
San Diego, CA 92121

Science Applications  
International Corporation  
Attn: Michael B. Gross  
Ass't. Vice President  
Suite 1250  
160 Spear Street  
San Francisco, CA 94105

Systems, Science, and Software (2)  
Attn: E. Peterson  
Box 1620  
La Jolla, CA 92038

Westinghouse Electric Corporation (7)  
Attn: Library  
Lamar Trego  
W. P. Poirer  
W. R. Chiquelin  
V. F. Likar  
D. J. Moak  
R. F. Kehrman  
P.O. Box 2078  
Carlsbad, NM 88221

Weston Corporation (1)  
Attn: David Lechel  
Suite 1000  
5301 Central Avenue, NE  
Albuquerque, NM 87108

#### UNIVERSITIES

University of Arizona  
Attn: J. G. McCray  
Department of Nuclear Engineering  
Tucson, AZ 85721

University of British Columbia (2)  
Attn: R. A. Freeze  
J. L. Smith  
Department of Geological Sciences  
6339 Stores Road  
Vancouver, British Columbia V6T 2B4  
CANADA

University of New Mexico (2)  
Geology Department  
Attn: Library  
Albuquerque, NM 87131

Pennsylvania State University  
Materials Research Laboratory  
Attn: Della Roy  
University Park, PA 16802

Texas A&M University  
Center of Tectonophysics  
College Station, TX 77840

G. Ross Heath  
College of Ocean  
and Fishery Sciences  
University of Washington  
Seattle, WA 98195

University of Virginia  
Attn: G. M. Hornberger  
Department of Environmental Sciences  
Clark Hall  
Charlottesville, VA 22903

#### INDIVIDUALS

Dennis W. Powers  
Star Route Box 87  
Anthony, TX 79821

#### LIBRARIES

Thomas Brannigan Library  
Attn: Don Dresp, Head Librarian  
106 W. Hadley St.  
Las Cruces, NM 88001

Hobbs Public Library  
Attn: Ms. Marcia Lewis, Librarian  
509 N. Ship Street  
Hobbs, NM 88248

New Mexico State Library  
Attn: Ms. Ingrid Vollenhofer  
P.O. Box 1629  
Santa Fe, NM 87503

New Mexico Tech  
Martin Speere Memorial Library  
Campus Street  
Socorro, NM 87810

Pannell Library  
Attn: Ms. Ruth Hill  
New Mexico Junior College  
Lovington Highway  
Hobbs, NM 88240

WIPP Public Reading Room  
Attn: Director  
Carlsbad Public Library  
101 S. Halagueno St.  
Carlsbad, NM 88220

Government Publications Department  
General Library  
University of New Mexico  
Albuquerque, NM 87131

THE SECRETARY'S BLUE RIBBON PANEL  
ON WIPP

Dr. Thomas Bahr  
New Mexico Water Resources Institute  
New Mexico State University  
Box 3167  
Las Cruces, NM 88003-3167

Mr. Leonard Slosky  
Slosky and Associates  
Suite 1400  
Bank Western Tower  
1675 Tower  
Denver, CO 80202

Mr. Newal Squyres  
Holland & Hart  
P.O. Box 2527  
Boise, ID 83701

Dr. Arthur Kubo  
Vice President  
BDM International, Inc.  
7915 Jones Branch Drive  
McLean, VA 22102

Mr. Robert Bishop  
Nuclear Management Resources Council  
Suite 300  
1776 I Street, NW  
Washington, DC 20006-2496

NATIONAL ACADEMY OF SCIENCES,  
WIPP PANEL

Dr. Charles Fairhurst, Chairman  
Department of Civil and  
Mineral Engineering  
University of Minnesota  
500 Pillsbury Dr., SE  
Minneapolis, MN 55455

Dr. John O. Blomeke  
Route 3  
Sandy Shore Drive  
Lenoir City, TN 37771

Dr. John D. Bredehoeft  
Western Region Hydrologist  
Water Resources Division  
U.S. Geological Survey (M/S 439)  
345 Middlefield Road  
Menlo Park, CA 94025

Dr. Karl P. Cohen  
928 N. California Avenue  
Palo Alto, CA 94303

Dr. Fred M. Ernsberger  
250 Old Mill Road  
Pittsburgh, PA 15238

Dr. Rodney C. Ewing  
Department of Geology  
University of New Mexico  
200 Yale NE  
Albuquerque, NM 87131

B. John Garrick  
Pickard, Lowe & Garrick, Inc.  
2260 University Drive  
Newport Beach, CA 92660

John W. Healy  
51 Grand Canyon Drive  
Los Alamos, NM 87544

Leonard F. Konikow  
U.S. Geological Survey  
431 National Center  
Reston, VA 22092

Jeremiah O'Driscoll  
505 Valley Hill Drive  
Atlanta, GA 30350

Dr. D'Arcy A. Shock  
233 Virginia  
Ponca City, OK 74601

Dr. Christopher G. Whipple  
Clement International  
Suite 1380  
160 Spear Street  
San Francisco, CA 94105

Dr. Peter B. Myers, Staff  
Director  
National Academy of Sciences  
Committee on Radioactive  
Waste Management  
2101 Constitution Avenue  
Washington, DC 20418

Dr. Geraldine Grube  
Board on Radioactive Waste  
Management  
GF456  
2101 Constitution Avenue  
Washington, DC 20418

Dr. Ina Alterman  
Board on Radioactive Waste  
Management  
GF462  
2101 Constitution Avenue  
Washington, DC 20418

#### FOREIGN ADDRESSES

Studiecentrum Voor Kernenergie  
Centre D'Energie Nucleaire  
Attn: Mr. A. Bonne  
SCK/CEN  
Boeretang 200  
B-2400 Mol  
BELGIUM

Mr. D. J. Pascoe  
Environment Canada  
Ontario Region/G&P  
25 St. Clair Avenue East  
Toronto, Ontario M4T 1M2  
CANADA

Atomic Energy of Canada, Ltd. (2)  
Whiteshell Research Estab.  
Attn: Peter Haywood  
John Tait  
Pinewa, Manitoba, CANADA  
ROE 1LO

Dr. D. K. Mukerjee  
Ontario Hydro Research Lab  
800 Kipling Avenue  
Toronto, Ontario, CANADA  
M8Z 5S4

Mr. Francois Chenevier, Director (2)  
ANDRA  
Route du Panorama Robert Schumann  
B.P.38  
92266 Fontenay-aux-Roses Cedex  
FRANCE

OECD Nuclear Energy Agency (3)  
Attn: Dr. Hong L. Chang  
Dr. Daniel A. Galson  
Mr. Jean-Pierre Olivier  
Division of Radiation Protection  
and Waste Management  
38, Boulevard Suchet  
75016 Paris, FRANCE

Claude Sombret  
Centre D'Etudes Nucleaires  
De La Vallee Rhone  
CEN/VALRHO  
S.D.H.A. BP 171  
30205 Bagnols-Sur-Ceze  
FRANCE

Gesellschaft fur Reaktorsicherheit  
Attn: Peter Bogorinski  
Schwertnergasse 1  
500 Koln 1  
FEDERAL REPUBLIC OF GERMANY

Bundesministerium fur Forschung und  
Technologie  
Postfach 200 706  
5300 Bonn 2  
FEDERAL REPUBLIC OF GERMANY

Bundesanstalt fur Geowissenschaften  
und Rohstoffe  
Attn: Michael Langer  
Postfach 510 153  
3000 Hannover 51  
FEDERAL REPUBLIC OF GERMANY

Hahn-Meitner-Institut fur Kernforschung  
Attn: Werner Lutze  
Glienicke Strasse 100  
100 Berlin 39  
FEDERAL REPUBLIC OF GERMANY

Institut für Tieflagerung (4)  
Attn: K. Kuhn  
Theodor-Heuss-Strasse 4  
D-3300 Braunschweig  
FEDERAL REPUBLIC OF GERMANY

Kernforschung Karlsruhe  
Attn: K. D. Closs  
Postfach 3640  
7500 Karlsruhe  
FEDERAL REPUBLIC OF GERMANY

Physikalisch-Technische Bundesanstalt  
Attn: Peter Brenneke  
Postfach 33 45  
D-3300 Braunschweig  
FEDERAL REPUBLIC OF GERMANY

D. R. Knowles  
British Nuclear Fuels, plc  
Risley, Warrington, Cheshire WA3 6AS  
1002607 GREAT BRITAIN

Shingo Tashiro  
Japan Atomic Energy Research Institute  
Tokai-Mura, Ibaraki-Ken  
319-11 JAPAN

Netherlands Energy Research Foundation  
ECN (2)  
Attn: Tuen Deboer, Mgr.  
L. H. Vons  
3 Westerduinweg  
P.O. Box 1  
1755 ZG Petten, THE NETHERLANDS

Svensk Kärnbränsleforsörjning AB  
Attn: Fred Karlsson  
Project KBS  
Kärnbränslesakerhet  
Box 5864  
10248 Stockholm, SWEDEN

KEMAKTA Consultants Co.  
Attn: Mark Elert  
Pipersgatan 27  
S-112 28  
Stockholm  
SWEDEN

SANDIA INTERNAL

400 L. D. Tyler  
1511 D. F. McTigue  
1514 C. M. Stone  
3141 S. A. Landenberger (5)  
3151 Supervisor (3)  
3154-1 C. L. Ward, (10) for DOE/OSTI  
6000 V. L. Dugan, Acting  
6232 W. R. Wawersik  
6233 R. T. Cygan  
6300 T. O. Hunter, Acting  
6310 T. E. Blejwas, Acting  
6313 L. E. Shephard  
6313 R. J. Glass  
6340 W. D. Weart  
6340 S. Y. Pickering  
6340A A. R. Lappin  
6341 R. C. Lincoln  
6341 Staff (9)  
6341 Sandia WIPP Central Files (10)  
6342 D. R. Anderson  
6342 Staff (11)  
6343 T. M. Schultheis  
6343 Staff (2)  
6344 E. D. Gorham  
6344 P. B. Davies (30)  
6344 Staff (10)  
6345 B. M. Butcher, Acting  
6345 Staff (9)  
6346 J. R. Tillerson  
6346 Staff (7)  
7223 C. A. Gotway  
8524 J. A. Wackerly (SNLL Library)  
9300 J. E. Powell  
9310 J. D. Plimpton  
9320 M. J. Navratil  
9325 L. J. Keck (2)  
9330 J. D. Kennedy  
9333 O. Burchett  
9333 J. W. Mercer  
9334 P. D. Seward

Dist-8